

SURFACE PLASMON-ENHANCED LIGHT EMISSION  
FROM ORGANIC LIGHT EMITTERS

Thesis by

Terrell D. Neal

In Partial Fulfillment of the Requirements

for the Degree of

Doctor of Philosophy

California Institute of Technology

Pasadena, California

2006

(Defended May 30, 2006)

© 2006

Terrell D. Neal

All Rights Reserved

## Acknowledgements

## Abstract

1	Introduction.....	1
2	Background.....	6
2.1	Surface Plasmons.....	6
2.2	Dispersion Relation.....	6
2.3	Conjugated Polymers.....	8
2.4	References.....	10
3	Surface Plasmon Enhanced Emission from Dye Doped Polymer Layers	
3.1	Abstract.....	13
3.2	Introduction.....	14
3.3	Experiment.....	15
3.4	Results and Discussion.....	19
3.5	Conclusions.....	24
3.6	References.....	25
4	Time Resolved Photoluminescence Spectroscopy of Surface Plasmon Enhanced Emission from Conjugated Polymers	
4.1	Abstract.....	27
4.2	Introduction.....	28
4.3	Experiment.....	28
4.4	Results and Discussion.....	33
4.5	Conclusion.....	36
4.6	References.....	37
	Unifying summary.....	38
5	Nanofabricated Devices and Applications	
5.1	Metal Nanostructures on Insulator.....	40
5.2	Experimental Procedures.....	40
5.3	Results and Discussion.....	43
5.4	DNA Conductivity.....	47
5.5	Nanostructured Insulator for Metal Nanoparticle Analysis Device.....	48
5.6	Conclusion.....	49
5.7	References.....	50
6	Mask Pattern Transferred Transient Grating Technique	
6.1	Abstract.....	51
6.2	Introduction.....	52
6.3	Method.....	53
6.4	Experimental.....	57
6.5	Results and Discussion.....	58
6.6	Conclusion.....	64
6.7	References.....	65
7	Molecular Filter-Nanosieve	
7.1	Abstract.....	67
7.2	Introduction.....	68
7.3	Theory.....	68

7.4	Experimental .....	69
7.5	Results and Discussion .....	71
7.6	Conclusion .....	71
7.7	Reference .....	72
8	Photo-oxidation competes with surface plasmon coupling	
8.1	Abstract .....	73
8.2	Introduction.....	74
8.3	Experiment.....	74
8.4	Results and Discussion .....	75
8.5	Conclusion .....	76
8.6	References.....	80
9	Geometry in sync with surface plasmon coupling	
9.1	Abstract .....	81
9.2	Introduction.....	82
9.3	Experiment.....	82
9.4	Results and Discussion .....	86
9.5	References.....	90
	Conclusion .....	91
	Appendices	
	Appendix A.....LED Trend.....	92
	Appendix B.....Laser Dyes .....	93
	Appendix C.....Experimental Setup .....	95
	Appendix D.....Conjugated Polymers .....	96
	Appendix E.....Surface Plasmon Coupling Mechanism and Dispersion Diagram..	100

# List of Figures

## Chapter 3

Figure 1 Sample structure with both pump light and emission light configurations.

Figure 2 PL spectra of Coumarin 460 on Ag, Au, and on no metal. Coumarin 460 PL spectra on no metal was normalized to 1.

Figure 3 PL Enhancement ratios demonstrating an increase of enhancement with shorter wavelengths using the silver film. Green dotted line is for gold whereas red solid line is for silver.

Figure 4 Dispersion diagrams of surface plasmons generated on Ag/PMMA red solid line and Au/PMMA green dotted line.

## Chapter 4

Figure 1 Molecular structures for (a) pf1cnp1, (b) pf3cnp1, (c) and pftpaq.

Figure 2 PL enhancements, (a) pf1cnp1, (b) pf3cnp1, (c) pftpaq and (d) enhancement ratios plotted against the wavelength.

Figure 3 TRPL with the data normalized to 1 where the dotted line shows the conjugated polymer carrier decay rate with metal and solid line without metal, (a) pf1cnp1, (b) pf3cnp1, (c) pftpaq.

Figure 4 Carrier lifetime plotted against the wavelength (a) pf1cnp1, (b) pf3cnp1, and (c) pftpaq. Average Purcell factor for the conjugated polymers studied.

## Chapter 5

Figure 1 (a) Corrugated pattern in PMMA, on Au, on PMMA, on quartz. (b) Cartoon of layered structure, where the middle layer is the sandwiched Au between PMMA layers and an example pattern are shown.

Figure 2 Fabrication steps to obtain metal-filled trenches within a sample.

Figure 3 Optical microscope image of gold-filled corrugated trench in quartz.

Figure 4 Corrugated wire structures at various stages of fabrication.

Figure 5 Images showing the quality of the structures.

Figure 6 Images of arrays of electron beam written patterns of different specifications.

Figure 7 Images of gold corrugated lines with contact pads and cartoon of structure.

Figure 8 Proposed isolated gold mounds on graphite sample schematic.

Figure 9 Mask design for making the structure and schematic of structure.

Figure 10 Schematic of nanostructure sample.

Figure 11 Optical microscope image of channels in metal on quartz.

## Chapter 6

Figure 1 Pump and probe beams alignments for (a) traditional optical heterodyne detected-transient grating (OHD-TG) technique and (b) the present mask pattern transferred-transient grating (MPT-TG) technique.

Figure 2 Schematic diagram of the permanent metal grating and induced spatial modulation of light intensity. Spiropyran molecules were photoexcited and transformed from merocyanine form (MF) to spiro form (SP) along the bright-dark pattern.

Figure 3 Time profiles of the diffracted signals (TG signals) in microsecond timescale (a) and millisecond timescale (b). The dashed lines denote the initial intensities of the reference beam ( $I_r$ ).

Figure 4 Semi-log plots of the TG signals in microsecond timescale (a) and in millisecond timescale (b). The straight lines are best fits.

## **Chapter 7**

Figure 1 Illustration of nanosieve, left, and close-up on the right, with a thin gold film evaporated on both sides of the substrate. (Layers not drawn to scale.)

Figure 2 SEM view of e-beam-written, etched holes and alignment mark used for offsetting the top layer.

Figure 3 Suspended epi-Si membrane with e-beam-written holes in the center.

## **Chapter 8**

Figure 1 Surface Plasmon Effect without nitrogen flowing.

Figure 2 Nitrogen Effect illustrating the PL intensity decay of the conjugated polymer on bare quartz with nitrogen flowing.

Figure 3 Surface Plasmon Effect and Nitrogen Effect.

## **Chapter 9**

Figure 1 Cartoon illustration of the fabrication process for the entrenched metal grating structures.

Figure 2 Entrenched grating structures before (above) and after liftoff (below).

Figure 3 Peak PL intensities of the conjugated polymer on the entrenched metal gratings fabricated.

Figure 4 Peak PL intensities of the conjugated polymer on the surface mounted metal gratings fabricated (normalized).

## **Acknowledgements**

This thesis is for my parents and all of my family and friends.

With great humility I attempt to acknowledge those that have made this thesis possible.

I would like to also thank the well wishers all over the country that have met me with inspiring words with each encounter.

I am indeed thankful for the journey. In addition to what I have learned over these years, I am extremely happy for those whom I have had the opportunity to teach while a student.

Thanks to my many mentors at Morehouse College and Georgia Tech. Thanks to all the well wishers back home in GA. “Putting Warrenton on the map”. Thanks to my collaborator extraordinaire, Dr. Koichi Okamoto. I also appreciate the discussions with colleagues and friends: Zhaoyu Zhang, Yan Chen, Sandra Steinberg, Joe Zendejas, and Dr. Christopher Boxe.

I also thank the following: NASA Ronald E. McNair for undergraduate support and internships, AT&T for a summer research experience, Undergraduate Research Opportunities Program UROP at GA Tech, GEM Fellowship, David and Lucile Packard Foundation Fellowship, AAAS Graduate Scholars Program, and the MDITR Fellowship.

I thank my collaborators at the University of Washington, Prof. Alex Jen, and Dr. Michelle Liu and the CMDITR.

Thanks to the administrators for providing the opportunity to recruit and mentor in many capacities, allowing me to maintain the “whole student” status.

Thanks to Prof. Axel Scherer for the opportunity and freedom to explore.

## **Abstract**

We have experimentally verified that visible light emission for various organic light emitters can be enhanced through the use of surface plasmon coupling layers. By matching the plasmon frequency of a thin unpatterned silver film to the emission of a dye-doped polymer deposited onto this metal surface, we have observed an 11-fold enhancement of light emission. By patterning the silver layer, we estimate that the plasmon frequency can be tuned to match dye-doped polymer emission frequencies, and even larger emission enhancements as well as extraction efficiencies are expected. Carrier dynamics of such plasmon-enhanced organic light emitters were studied and a recombination rate increase due to surface plasmon polaritons was experimentally observed. Internal quantum efficiency data from the polyfluorenes studied follow the trend supported by the time-resolved photoluminescence measurements. Also, we have presented a way to extend the lifetime of organic light emitters by reducing the photodegradation effects from photo-oxidation using surface plasmon coupling.

## Chapter 1–Introduction

Three areas-nanotechnology, surface plasmons, and light-emitting devices-come together as the backbone of this thesis. Nanotechnology can be defined as the study or manipulation of things on the order of billionths of a meter in size. In the area of light emitting devices, the focus is drawn from vacuum tube technology to semiconductor devices to conducting polymers. The angle taken with surface plasmons is from theory to application. Nano-sized particles and structures are known to exhibit a strong interaction with light. We use nanotechnology to make and modify devices, specifically to enhance device capability. Therefore, it is not uncommon that we have a interweaving of topics in this thesis, since on the path to achieving new landmarks in science the research efforts are becoming more interdisciplinary. It is with that idea of pioneering areas that this work is based.

This introduction chapter briefly outlines the work carried out in the subsequent chapters of this thesis. The interdisciplinary nature of this thesis calls for a background of a couple of areas that are each given adequate attention in Chapter 2. One main hurdle to overcome when working on topics that span several disciplines is language. In the effort detailed in this thesis, we lean more toward the applied physicist and engineering way of looking at things when describing all the topics covered.

The work discussed in Chapter 3 has already gained attention of readers in the magazine *Laser Focus World*,<sup>1</sup> where the work detailing surface plasmon enhanced light emission from dye-doped polymer layers is featured. We explore methods to enhance the light

emission from dye-doped polymer layers by using surface plasmon coupling to thin metal films. Commercial laser dyes were doped into a host polymer, polymethylmethacrylate (PMMA). Also, more intensive studies studying the size dependent photoluminescence of silver nanoparticles doped in PMMA have been inspired by my work.<sup>2</sup>

In Chapter 4 we continue looking into the effect of emission intensity enhancements of organic light emitters due to surface plasmons coupling to light. Having noticed the impact of OLEDs as well as being aware of some of their high internal quantum efficiencies, we decided that the material used to make them should be candidates for this study. The carrier dynamics, mainly the lifetime of the carriers, are also compared.

While some researchers search for new architectures to achieved high efficiency organic light-emitting diodes,<sup>3</sup> others work on theoretically investigating the tuning the surface plasmons that couple spontaneously from emitted photons to increase the efficiency of light-emitting devices.<sup>4</sup> Indeed, some theoretical and experimental work has been pursued to extract more light from polymer light-emitting diodes.<sup>5</sup> Citrin recently published an article of interest that presents a possible theory for plasmon polaritons in nanoparticle chains within a gain medium for the possibility of using the gain to counterbalance dissipation and achieve low attenuation plasmon polaritons in nanoparticle chains.<sup>6</sup> The work by Citrin also supports the theme of the work discussed in Chapter 3.

In Chapter 5 we revisit nanofabricated devices and their applications, which set the theme for the research carried out in Chapters 3, 4, 6, and 7. Chapter 5 contains projects covered at some point during my graduate career. It was with these projects that a certain

level of expertise was attained. Most of the projects were fabrication intensive, involving many lithography steps. However, the technology behind making the devices was directly applicable to several areas. A nanostructured insulating substrate, as describe in the chapter, was useful in most cases where control of the analysis of nanoparticles or analysis performed with nanowires defined on the substrate was desired.

On the other hand, the fruit of the labor came in the form of the research topics explored thereafter. For instance, for the work in Chapter 7 we describe a method to have dynamic control over the size of particles filtered. Conventional methods of lithographically defining holes for the filter size are combined with advantages from thin film depositions.

Moreover, the skills of nanofabrication were directly applicable for a new technique in the class of optical heterodyne detected transient grating that is presented in Chapter 6. This technique, mask pattern transferred transient grating, is a convenient new technique to study chemical reactions and molecular dynamics. It is expected that the application of this simpler technique is not limited to chemistry and will span other science disciplines.

Chapters 3<sup>7</sup>, 6<sup>8</sup>, and 7<sup>9</sup> are published works, whereas Chapter 4 has been submitted for publication. Chapter 5 simply consists of unpublished works.

Chapter 8 came as a result of observation made during the exploration of topics covered in Chapters 3 and 4. In Chapter 8, we demonstrate a way to extend the lifetime of organic light emitters by reducing the photodegradation effects from photo-oxidation using surface plasmon coupling.

Further work can be done to identify methods in which to tune the geometry of metals in order to maximize the surface plasmon coupling. In Chapter 9, we investigate grating structures both within and on a substrate by photoluminescence measurements of the conjugated polymer placed on the samples. We observe emission intensity enhancements due to surface plasmon coupling.

Last but not least, conclusions containing mainly the big picture of the accomplishments of the work discussed are listed at the end of this thesis. Supporting materials are found in the Appendix.

**References**

1. Wallace, J. "Surface plasmons boost emission from dyed polymer," *Laser Focus World*, September 2005.
2. Basak, D., Karan, S., and Mallik, B., *Chem. Phys. Lett.* 420 (2006) 115–119.
3. Kim, H., Horwitz, J.S., Kim, W.H., Kafafi, Z.H., and Chrisey, D.B., *Journal of Appl. Phys.*, 91, 8, 2002.
4. Paiella, R., *Appl. Phys. Lett.*, 87, 111104 2005.
5. Ziebarth, J. M., McGehee, M.D., *Journal of Appl. Phys.*, 97, 064502, 2005.
6. Citrin, D.S., *Opt. Lett.*, 31, 98–100, 2006.
7. Neal, T.D., Okamoto, K., Scherer, A., *Optics Express*, 13, 14, 5522–5527, 2005.
8. Neal, T.D., Okamoto, K., Liu, M.S., Jen, A.K-Y, Scherer, A., Chu, C-F., *Submitted* 2006.
9. Okamoto, K., Neal, T.D., Zhang, Z., Wei, D.T., Scherer, A., *Chem. Phys. Lett.*, 414, 155–160, 2005.

## Chapter 2–Background

### Surface plasmons

We commence this study by exploring the physics of surface plasmons, electromagnetic surface waves that have their intensity maximum in the surface and exponentially decaying fields perpendicular to it. The oscillations of the electric field encounters the surface charge of the metal and essentially yields these trapped electromagnetic fields between the metal and the dielectric.

Researchers have developed methods to observe<sup>1</sup> and have intensively studied the surface plasmon polaritons<sup>2</sup> and examined the nature of the surface plasmon-polariton modes and how the energy lost to the modes can be recovered when light-emission sources are in close proximity to a thin metallic film. Also, the ability to design the surface plasmon modes has been proposed<sup>3</sup> and experimentally verified.<sup>4</sup>

### Dispersion Relation

The dispersion relation<sup>5</sup> relates the frequency of surface plasma oscillations to its wave vector. We can describe the field by

$$E = E_0^{\pm} \exp[+i(k_x x \pm k_z z - \omega t)] \quad 2.1$$

with + for  $z \geq 0$ , - for  $z \leq 0$ , and with imaginary  $k_z$ , which causes the exponential decay of the field  $E_z$ . The wave vector  $k_x$  lies parallel to the x direction;  $k_x = 2\pi / \lambda_p$ , where  $\lambda_p$  is the wavelength of the plasma oscillation. Maxwell's equations yield the retarded

dispersion relation for the plane surface of a semi-infinite metal with the dielectric function ( $\varepsilon_1 = \varepsilon_1' + i\varepsilon_1''$ ), adjacent to a medium  $\varepsilon_2$  as air or vacuum:

$$D_0 = \frac{k_{z1}}{\varepsilon_1} + \frac{k_{z2}}{\varepsilon_2} = 0 \quad 2.2$$

$$\varepsilon_i \left( \frac{\omega}{c} \right)^2 = k_x^2 + k_{zi}^2 \quad \text{or} \quad 2.3$$

$$k_{zi} = \left[ \varepsilon_i \left( \frac{\omega}{c} \right)^2 - k_x^2 \right]^{1/2}, \quad i=1, 2.$$

$$k_x = \frac{\omega}{c} \left( \frac{\varepsilon_1 \varepsilon_2}{\varepsilon_1 + \varepsilon_2} \right)^{1/2} \quad 2.4$$

Surface plasmons (SPs) are excited by the interaction between light and metal surfaces.<sup>5-6</sup> SPs, known to enhance absorption of light in molecules,<sup>7</sup> increase Raman Scattering intensities and light transparencies,<sup>8-9</sup> and also generate photonic band gap.<sup>12-13</sup> Since 1990, SPs have also received much attention when used in inorganic and organic light emitters.<sup>14-23</sup> Gianordoli et al. optimized the emission characterizations of GaAs-based LEDs by SPs.<sup>18</sup> Vuckovic et al. reported the SP-enhanced LED analyzing by both theoretically and experimentally.<sup>19</sup> Thus, great attention has been focused on SP enhanced emission. Other avenues in this field of research became apparent when Hobson et al. reported the SP-enhanced organic LEDs.<sup>20</sup> For InGaN QWs, Gontijo and co-workers report the coupling of the spontaneous emission from QW into the SP on silver thin film and showed increased absorption of light and the SP frequency.<sup>21</sup> Neogi et al. confirmed that the recombination rate in an InGaN/GaN QW could be significantly

enhanced by the time-resolved PL measurement.<sup>22</sup> However, in the aforementioned work, light could not be extracted efficiently from the silver/GaN surface. Therefore, the actual photoluminescence (PL) enhancement of InGaN/GaN by coupling into SP had not been observed directly until Okamoto and co-workers reported for the first time large PL increases from InGaN/GaN QW material coated with metal layers.<sup>23</sup>

### **Conjugated polymers**

The 2000 Nobel Prize in Chemistry was awarded to Alan J. Heeger, Alan G. MacDiarmid, and Hideki Shirakawa for work on polyacetylene, an organic polymer that can be converted to a conducting polymer. Since that discovery, a tremendous amount of work has been done on conjugated polymers, because of their ability to exhibit high conductivity when doped. A conjugated polymer is a carbon-based macromolecule through which valence  $\pi$ -electrons are delocalized. The electronics industry finds a particular interest in conjugated polymers for their electronic, optical, and mechanical properties as well as the intrinsic processing advantages that makes room for a wide array of applications, including but not limited to light-emitting devices, photovoltaic devices, electromagnetic shielding, plastic field-effect transistors, and nonlinear optical devices.<sup>24</sup> Some structural studies<sup>25</sup> represent some of the challenges that one encounters when attempting to understand the physical properties of such polymers. Many opportunities already exist for electrically conductive organic polymers, as studies<sup>26</sup> have been done to identify strong candidates for spacecraft materials, in reference to the thermal stability, radiation resistance, and strength of the polymer. Still there is much to find out about the relationship between the molecular structure and the conductivity.

Researchers find it possible to understand the polymer properties further by using time resolved photoluminescence studies to characterize conjugated polymers.<sup>27,28</sup>

Quite an effort has been place in the efficiencies and electron transporting properties of the polymers.<sup>29-31</sup>

**References**

1. Giannattasio, A., Barnes, W.L., Optics Express, 13, 2, 2005
2. Wedge, S., Barnes, W.L., Optics Express, Vol. 12, No. 16, 2004
3. Pendry, J.B., Martin-Moreno, L., Garcia-Vidal, F.J., Science 305, 847, 2005.
4. Hibbins, A.P., Evans, B.R., Sambles, J.R., Science, 308, 670, 2005.
5. Raether, H., *Surface plasmon on smooth and rough surfaces and on grating*, Springer, Berlin, 1988.
6. Liebsch, A., *Electronic Excitations at Metal Surfaces, Physics of Solids and Liquids*, Ansgar, Libsch, 1997.
7. Ford, G.W., and Weber, W.H., "Electromagnetic-interactions of molecules with metal-surfaces," Phys. Rep. 113, 195–287, 1984.
8. Fleischmann, M., Hendra, P.J., and McQuillan, A. J., "Raman spectra of pyridine adsorbed at a silver electrode," Chem. Phys. Lett. 26, 163–166, 1974.
9. Garcia-Vidal, J.F., and Pendry, J.B., "Collective theory for surface enhanced Raman scattering," Phys. Rev. Lett. 77, 1163–1166, 1996.
10. Ebbesen, T.W., Lezec, H.J., Ghasemi, H.F., Thio, T., and Wolff, P.A., "Extraordinary optical transmission through sub-wavelength hole arrays," Nature, 391, 667–669, 1998.
11. Schroter, U., and Heitmann, D., "Surface-plasmon-enhanced transmission through metallic gratings," Phys. Rev. B, 58, 15419–15421, 1998.
12. Kitson, S.C., Barnes W.L., and Sambles, J.R.A., "Full photonic band gap for surface modes in the visible," Phys. Rev. Lett. 77, 2670–2673, 1996.
13. Barnes, W.T., Preist, T.W., Kitson, S.C., and Sambles, J.R., "Physical origin of photonic energy gap in the propagation of surface plasmon on grating," Phys. Rev. B. 54, 6227–6244, 1996.
14. Kock, A., Gornik, E., Hauser, M., and Beinstingl, M., "Strongly directional emission from AlGaAs/GaAs light-emitting diode," Appl. Phys. Lett. 57, 2327–2329, 1990.
15. Hecker, N.E., Hopfel, R.A., and Sawaki, N., Physica E, "Enhanced light emission from a single quantum well located near a metal coated surface," 2, 98–101, 1998.

16. Hecker, N.E., Hopfel, R.A., and Sawaki, N., Maier, T., Strasser, G., "Surface plasmon-enhanced photoluminescence from a single quantum well," *Appl. Phys. Lett.* 75, 1577–1579, 1999.
17. Barnes, W.L., "Electromagnetic crystals for surface plasmon polaritons and the extraction of light from emissive devices," *J. Light. Tech.*, 17, 2170–2182, 1999.
18. Gianordoli, S., Hainberger, R., Kock, A., Finger, N., Gornik, E., Hank, C., and Korte, L., "Optimization of the emission characteristics of light emitting diodes by surface plasmons and surface waveguide modes," *Appl. Phys. Lett.* 77, 2295–2297, 2000.
19. Vuckovic, J., Loncar, M., Scherer, A., "Surface plasmon enhanced light-emitting diode," *IEEE J. Quant. Elec.* 36, 1131–1144, 2000.
20. Hobson, P.A., Wedge, S., Wasey, J.A.E., Sage, I., and Barnes, W.L., "Surface plasmon mediated emission from organic light emitting diodes," *Advanced Materials*, 14, 1393–1396, 2002.
21. Gontijo, I., Borodisky, M., Yablonovitch, E., Keller, S., Mishra, U.K., DenBaars, S.P., "Enhancement of spontaneous recombination rate in a quantum well by resonant surface plasmon coupling," *Phys. Rev. B*, 60, 11564–11567, 1999.
22. Neogi, A., Lee, C.-W., Everitt, H.O., Kuroda, T., Tackeuchi, A., Yablonovitch, E., "Enhancement of spontaneous recombination rate in a quantum well by resonant surface plasmon coupling," 66, 153305, 2002.
23. Okamoto, K., Niki, I., Shvartser, A., Narukawa, Y., Mukai, T., Scherer, A., "Surface-plasmon-enhanced light emitters based on InGaN quantum wells," *Nature Mater.*, 3, 601–605, 2004.
23. Barford, W., *Electronic and optical properties of conjugated polymers*, Oxford University Press Inc., New York, 2005.
24. Pouget, J.P., Robin, P. Comes, R., Gibson, H.W., Epstein, A.J., Billaud, D., *Physica*, 127 B, 158, 1984.
25. Cotts, D. B., and Reyes, Z., "Electrically conductive organic polymers for advanced applications," Noyes Data Corporation, New Jersey 1986.
26. Whitelegg, S.A., Buckley, A., Rahn, M.D., Fox, A.M., Bradley, D.D.C., Palsson, L.O., Samuel, I.D.W., Webster, G.R., Burn, P.L., *Synthetic Metals*, 119, 575–576, 2001.
27. Keivanidis, P. E., Jacob, J., Oldridge, L., Sonar, P. Carbonnier, B., Balushev, S., Grimsdale, A.C., Mullen, K., and Wegner, G., *ChemPhysChem*, 6, 1650–1660, 2005.

28. M. S. Liu, X. Jiang, P. Herguth, and A. K-Y. Jen, *Chem. Mater.*, 13, 3820–3822, 2001.
29. C-F. Shu, R. Dodda, F-I. Wu, M. S. Liu, and A. K-Y. Jen, *Macromolecules*, 36, 6698–6703, 2003.
30. Wu, F-I., Reddy, D.S., Shu, C-F., *Chem. Mater.*, 15, 269–274, 2003.

## **Chapter 3–Surface plasmon-enhanced emission from dye-doped polymer layers**

**Abstract:** We have experimentally verified that the emission of visible light from dye-doped polymers can be enhanced with the use of surface plasmon coupling. By matching the plasmon frequency of a thin unpatterned silver film to the emission of a dye-doped polymer deposited onto this metal surface, we have observed an eleven-fold enhancement of light emission. By patterning the silver layer, we estimate that the plasmon frequency can be tuned to match dye-doped polymer emission frequencies, and even larger emission enhancements as well as extraction efficiencies are expected.

## Introduction

The large optical fields provided by surface plasmons have in the past been used to increase significantly the fluorescence and luminescence intensity of dye molecules for applications in biological and biochemical sensing. Molecules can be detected on the surface of metal films or in close proximity to colloidal metal particles by measuring increases in the resonant surface plasmon coupled emission.<sup>1</sup> Recently, it has also been shown that plasmon resonances provided by thin metal layers and metal gratings can be designed to increase the efficiency of solid state semiconductor light sources. In such structures, the surface plasmon resonance frequency is tuned to the semiconductor quantum well emission, and the light-emission intensity can be increased by over an order of magnitude as nonradiative recombination paths are bypassed through coupling of recombination energy into surface plasmon modes. It is therefore not surprising that similar energy transfer into surface plasmons can also be exploited in the design of more efficient organic light emitters. Recently, the mechanism for emission enhancement through coupling to surface plasmons has been analyzed for InGaN quantum wells.<sup>2</sup> Other enhancement efforts to increase the external quantum efficiencies and increasing the spontaneous emission rates, using surface plasmons, have been reported for semiconductor quantum wells.<sup>3-6</sup> Similar increases in the internal and external quantum efficiencies to those observed in InGaN quantum wells in close proximity to metal surfaces can be obtained from dye-doped organic thin films.

Polymers, appropriately doped with dye molecules, emitting in the visible spectrum provide stable sources of light for displays and illumination sources at a significantly lower cost than semiconductors. Organic light-emitting diodes<sup>7,8</sup> (OLEDs) may indeed

evolve as the most inexpensive alternatives to fluorescent light sources for large area solid state lighting. Thus, it is of both commercial and scientific interest to improve the internal quantum efficiencies of the polymer dyes within such light emitters, as well as to increase the light extraction efficiencies from such organic films. Indeed, the effect of surface plasmons on the light emission from polymer layers has recently been investigated by several groups.<sup>9-11</sup> Nanosensors using surface plasmon resonance as well as their applications in conjunction with dye-doped polymers or polymer thin films have also been explored.<sup>12-14</sup> Here, we focus on enhancing the light emission efficiency from organic thin films by using the surface plasmon resonance.

## **Experiment**

The experimental setup used to measure our samples is shown in Fig. 1. To ensure that only a small amount of the pump light is reflected into the detector, the pump source is introduced at a large incidence angle while the detector is located perpendicular to the sample. We employ an Ocean Optics spectrometer to measure the emission intensity of the organic dye layers. We compare the influence of gold and silver thin films on the light emission of a commonly used laser dye doped in a polymer by using this measurement system. Of course, the light-emitting material must be within a few hundred nanometers of the metal surface to benefit from surface plasmon enhancements. For semiconductor quantum wells, this is normally accomplished by growing a very thin spacer separating the quantum well from the metal surface. For polymer layers, it is much simpler to prepare measurable samples, as it is only necessary to ensure that the pump light is not totally absorbed by the dye layer. Most plasmon enhancement

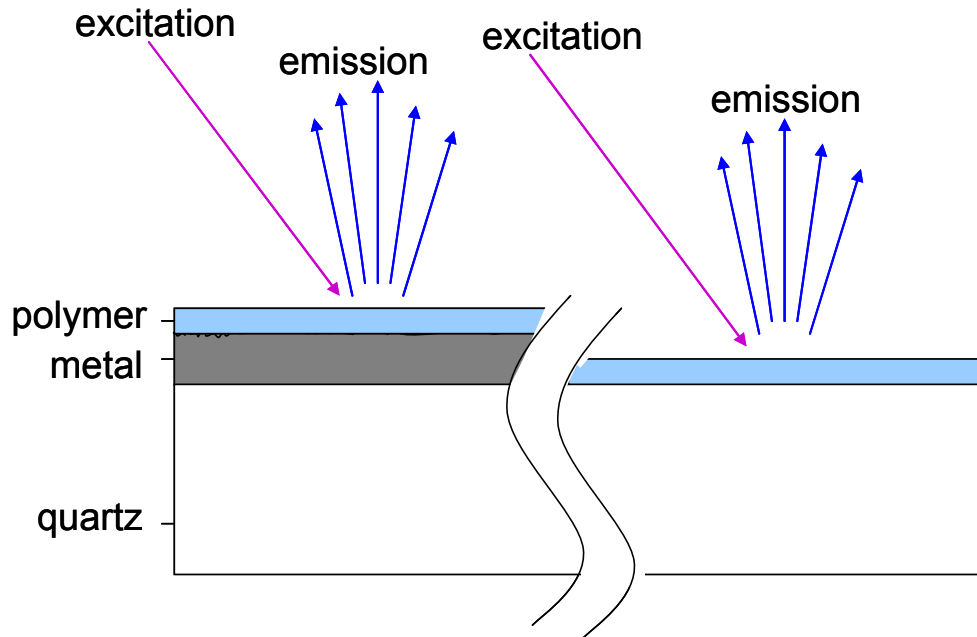


Fig. 1. Sample structure with both pump light and emission light configurations.

measurements conducted on semiconductor emitters have concentrated on backside pumping, through the sample, with the emission light measured also from the backside of the sample.<sup>2</sup> Some other work has measured the optical properties of semiconductors by topside pumping, through the metal, and measuring also from the top side.<sup>4,5</sup> Combinations of the different pumping and measurement configurations, as well as different angles for the pumped light, have also been pursued.<sup>6</sup> For this paper, it is most convenient to pump through the polymer as well as measure light from the polymer side of the sample.

It is of interest to control both the concentration of the dye material in the polymer as well as the thickness of the polymer. Dye polymer solution was prepared by dissolving common laser dye molecules of Coumarin 460 in chlorobenzene. This laser dye emits blue light at 460 nm with UV excitation. Then 2% polymethylmethacrylate (PMMA) was added to the mixture as a host matrix to obtain a 20 mM/L solution of the dye doped polymer solution. Photoluminescence measurements were performed by using a 405 nm InGaN laser diode to pump the Coumarin 460 dye. For the 405 nm pump light in Coumarin 460 the absorbance is  $0.633[10^{-4} \text{ dm}^3 \text{ mol}^{-1} \text{ cm}^{-1}]$ . Our concentration of  $2.16 \times 10^{-2}$  moles/L therefore results in an approximate excitation light penetration depth of  $\sim 646 \mu\text{m}$ , a penetration depth much larger than the sample thickness of 200 nm. To prepare the substrates for the dye-doped layers, 50 nm thick silver and gold layers were vapor deposited onto quartz substrates at 0.5 nm/second deposition rates. Gold and silver layers prepared under these conditions exhibit surface roughness of 30–40 nm resulting from the crystal size of the metal layers.<sup>2</sup> Only half of each substrate was metallized, enabling the rapid comparison between polymer emission on top of metal layers with polymer deposited on quartz. After the metallization step, the dye doped PMMA layers were spun onto both gold and silver substrates to obtain layer thicknesses of  $\sim 200$  nm.

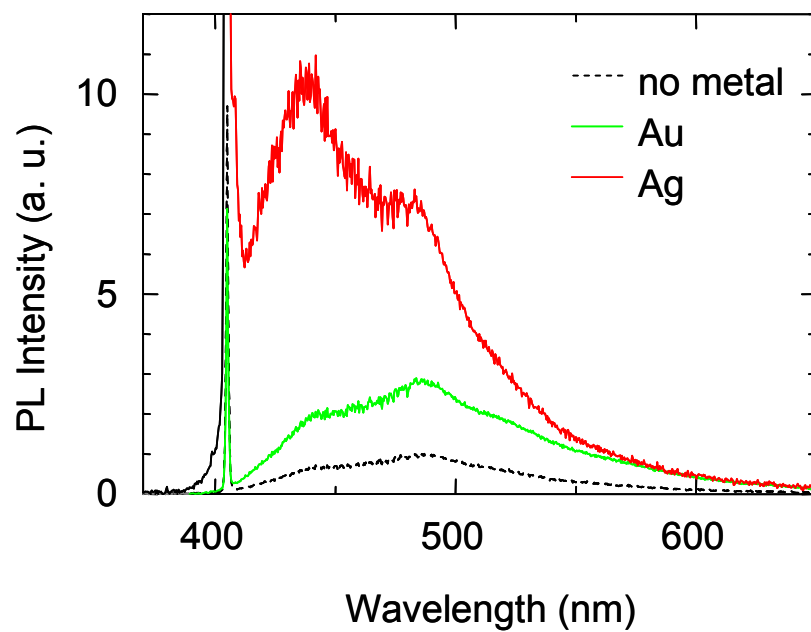


Fig. 2. PL spectra of Coumarin 460 on Ag, Au, and on no metal. Coumarin 460 PL spectra on no metal was normalized to 1.

## Results and Discussion

Figure 2 shows a typical measurement obtained when comparing the spectra of a region with Coumarin 460-doped PMMA spun onto gold with that of the polymer on the bare quartz substrate. While the gold assisted in reflecting the pump laser, the surface plasmons did not seem to couple to the emission wavelength of Coumarin 460 to offer any measurable enhancement. However, we do observe an 11-fold enhancement of the emission light from the Coumarin-doped PMMA on silver due the coupling of the surface plasmons generated on the silver film as the plasmon resonance frequency closely matches the emission frequency of the dye. Indeed, the dielectric constants for silver match well with the emission wavelength of Coumarin 460, and the data with the Coumarin 460 PL intensity is normalized to 1. While reflection can be used to account for some of the increased brightness, only the SP coupling can explain the enhancement measured.

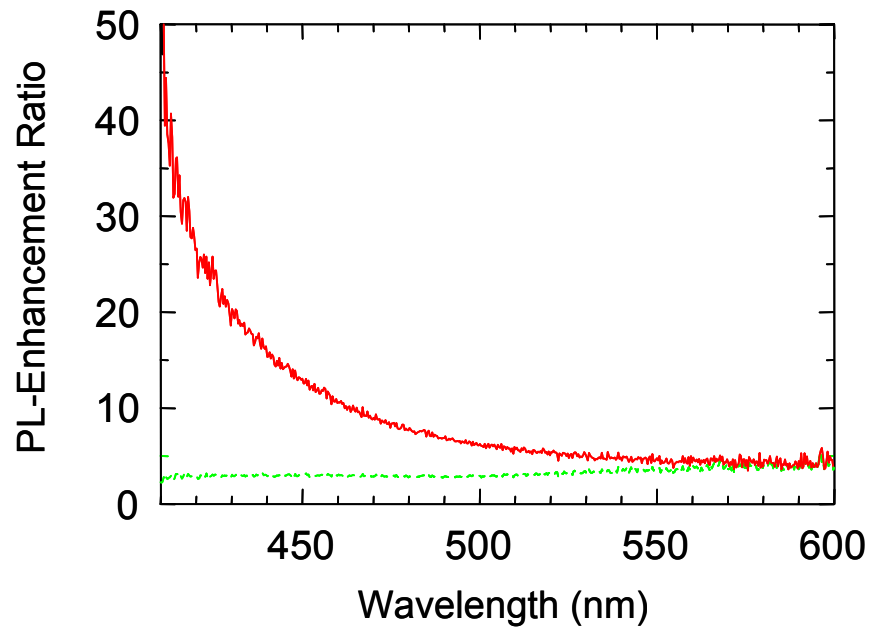


Fig. 3. PL Enhancement ratios demonstrating an increase of enhancement with shorter wavelengths using the silver film. Green dotted line is for gold whereas red solid line is for silver.

Enhancement ratios illustrated in Fig. 3 further support the notion of SP coupling between the silver and polymer interface. Up to 50 times the enhancement is observed along the broad emission spectrum of the dye-doped polymer whereas at the peak emission wavelength the photoluminescence enhancement ratio is 11 times. We observed an increase of photoluminescence enhancement ratio with shorter wavelengths for the silver film. However, the PL enhancement ratio is not strongly dependent on the change in wavelength for the gold film.

The dramatic PL enhancement of samples with Ag can be attributed to the strong interaction between the excited dye molecules and SPs. Electron-excited energy of molecules can couple to the electron vibration energy of SP. Then, the molecular relaxation processes may produce an SP instead of a photon, and this new path of the relaxation increases the spontaneous recombination rate. If the metal surface were perfectly flat, it would be difficult to extract light emission from the SP, since it is a non-propagating evanescent wave. However, roughness and imperfections in evaporated metal can scatter SPs as light. The coupling rate between the excited molecular and SP is expected to be much faster than the nonradiative relaxation processes as a result of the large electromagnetic fields introduced by the large density of states.

The phenomenon we exploit here heavily depends on the relationship of the metal dielectric function<sup>15</sup> and that of the polymer. The dielectric constant for PMMA is 2.6 at 1 MHz. The surface plasmon dispersion relationship is obtained by using the following equation to calculate the propagation wave number  $k$ :

$$k = \frac{\omega}{c} \sqrt{\frac{\epsilon_1 \epsilon_2}{\epsilon_1 + \epsilon_2}} \quad (1)$$

where  $\omega$  is the frequency,  $c$  is the speed of light, and  $\varepsilon_1, \varepsilon_2$  are the real parts dielectric constant of metal and PMMA, respectively. In this equation, the wave number  $k$  varies with frequency  $\omega$ . The plot of the surface plasmon dispersion relationship in Fig. 4 is calculated using Eq. (1).

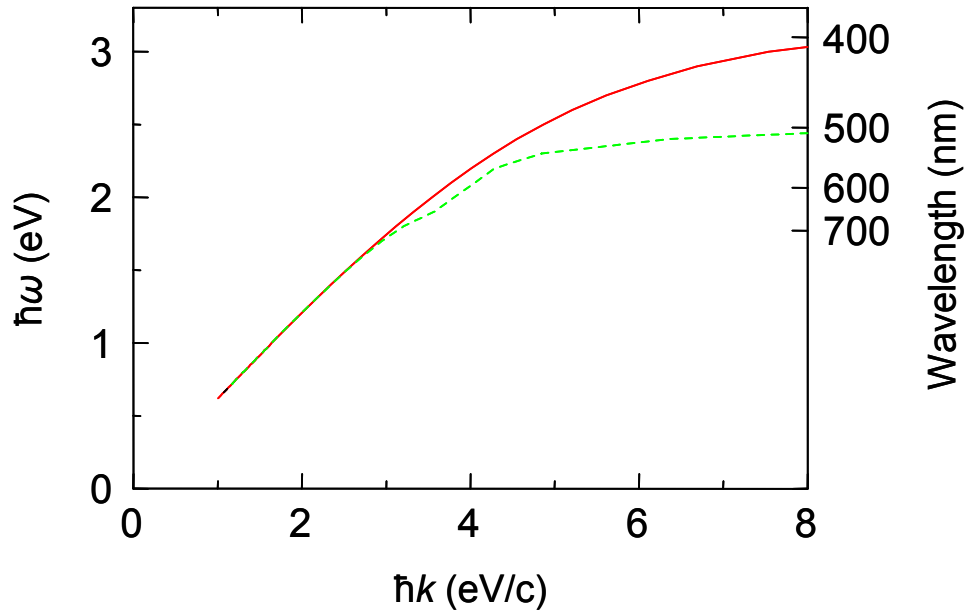


Fig. 4. Dispersion diagrams of surface plasmons generated on Ag/PMMA red solid line and Au/PMMA green dotted line.

The asymptotes of the Ag/PMMA and Au/PMMA surface plasmon dispersion curves closely approach the surface plasmon frequency for silver and gold, respectively. We can therefore determine the energy due to the coupling at the interface of the metal and the polymer. This provides a further explanation for the energy coupling exhibited in the laser dye-doped polymer deposited on different metallized substrates. Emission of the Coumarin 460 is closely aligned with the surface plasmon frequency for silver.

Usually, surface plasmons generated at the interface of the metal and the surrounding medium decay exponentially with distance from the metal surface. We can predict the surface plasmon penetration depth ( $Z$ ) in the polymer from the following equation:

$$Z = \frac{\lambda}{2\pi} \sqrt{\frac{\epsilon_2 - \epsilon_1}{\epsilon_1^2}} \quad (2)$$

This penetration depth is 38.6 nm for silver and 23.0 nm for gold, when we substitute the wavelength of the pump light  $\lambda$ . Therefore, since our penetration depth in the polymer due to the excitation wavelength and concentration of the dye molecules in the polymer was much longer than the penetration depths of the surface plasmons in the polymer, we could excite every part of the dye molecules adjacent to the metal.

Spacer dependency was explored by fabricating a new sample and first spinning on a 50 nm thick non-doped polymer layer and baking it at 180 °C to drive off the solvents. This layer was sandwiched between the metal film and the dye-doped polymer layer and lowered the coupling efficiency by not allowing efficient enhancement due to surface plasmons. This configuration placed the light-emitting material much farther away from the metal than the surface plasmon penetration depth mentioned above. Metal dependency trials performed showed that a thinner gold film, around 10 nm, had enhanced absorption while a thinner silver film, also 10 nm, did not enhance the signal. This result is reasonable based on previously reported calculations.<sup>5</sup>

## **Conclusions**

We have observed that the emission of dye-doped polymers can be enhanced by using surface plasmon coupling to thin metal layers. This study serves as a foundation for the geometric tuning of the surface plasmon resonance and enhancement of the emission of dye polymers using surface plasmons with patterned metal samples. If tuned properly, such lithographically structured layers should provide even higher enhancement values for the dye emission intensity. As the metallic surface can be used as an electrical contact, as a metallic grating for enhanced light extraction, and as a mirror for the definition of ultra-small optical cavities to further increase the spontaneous emission rates, we expect that many organic light-emitting diodes could benefit from careful design and choice of metallization. Ultimately, lithographic tuning of the peak emission wavelength and optimization of the polymer layer stack can also result in efficient white light source OLEDs.

## References

- <sup>1</sup>Malicka, J., et al., "Use of surface plasmon-coupled emission to measure DNA hybridization," *J. Biomol. Screening*, 9, 208–215, 2004.
- <sup>2</sup>Okamoto, K., et al., "Surface-plasmon-enhanced light emitters based on InGaN quantum wells," *Nature Materials*, 3, 601–605 2004.
- <sup>3</sup>Vuckovic, J., M. Loncar, and A. Scherer, "Surface plasmon enhanced light-emitting diode," *IEEE J. Quantum Electronics*, 36, 1131–1144, 2000.
- <sup>4</sup>Gontijo, I., et al., "Coupling of InGaN quantum-well photoluminescence to silver surface plasmons," *Phys. Rev. B*, 60, 11564–11567, 1999.
- <sup>5</sup>Neogi, A., et al., "Enhancement of spontaneous recombination rate in a quantum well by resonant surface plasmon coupling," *Phys. Rev. B*, 66, 2002.
- <sup>6</sup>Hecker, N.E., et al., "Surface plasmon-enhanced photoluminescence from a single quantum well," *Appl. Phys. Lett.*, 75, 1577–1579, 1999.
- <sup>7</sup>Jiang, X.Z., et al., "Organic light-emitting diodes using an in situ thermally polymerized hole transporting layer," *Appl. Phys. Lett.*, 76, 2985–2987, 2000.
- <sup>8</sup>Carlson, B., et al., "Divalent osmium complexes: Synthesis, characterization, strong red phosphorescence, and electrophosphorescence," *J. Am. Chem. Soc.*, 124, 14162–14172, 2002.
- <sup>9</sup>Hobson, P.A., et al., "Surface plasmon mediated emission from organic light-emitting diodes," *Advanced Materials*, 14, 1393–1396, 2002.
- <sup>10</sup>Andrew, P. and W.L. Barnes, "Energy transfer across a metal film mediated by surface plasmon polaritons," *Science*, 306, 1002–1005, 2004.
- <sup>11</sup>Alencar, M., A.S.L. Gomes, and C.B. de Araujo, "Directional laserlike emission from a dye-doped polymer containing rutile nanoparticles," *J. Opt. Soc. Am. B-Optical Physics*, 20, 564–567, 2003.
- <sup>12</sup>Uznanski, P. and J. Pecherz, "Surface plasmon resonance of azobenzene-incorporated polyelectrolyte thin films as an H<sup>+</sup> indicator," *J. Appl. Polymer Sci.*, 86, 1459–1464, 2002.
- <sup>13</sup>Tawa, K. and W. Knoll, "Out-of-plane photoreorientation of azo dyes in polymer thin films studied by surface plasmon resonance spectroscopy," *Macromol.*, 35, 7018–7023, 2002.

<sup>14</sup>Okamoto, T., T. Kamiyama, and I. Yamaguchi, "All-Optical Spatial Light-Modulator With Surface-Plasmon Resonance," *Opt. Lett.*, 18, 1570–1572, 1993.

<sup>15</sup>Carper, J., *The CRC Handbook of Chemistry and Physics*, Library Journal, 124, 192–+, 1999.

## **Chapter 4–Time-resolved photoluminescence spectroscopy of surface plasmon-enhanced light emission from conjugate polymers**

### **Abstract**

We have experimentally verified that the light emission from conjugated polymers can be enhanced through the use of surface plasmon coupling layers. Carrier dynamics of such plasmon-enhanced organic light emitters were studied and a recombination rate increase due to surface plasmon polaritons was experimentally observed. Internal quantum efficiency data from the polyfluorenes studied follow the trend supported by the time-resolved photoluminescence measurements.

## Introduction

Organic light-emitting diodes (OLEDs) have become widely available and are used for replacing inorganic light-emitting diodes, as they are less expensive and provide many opportunities in regards to structural placement. Despite the tremendous promise for efficient solid state lighting offered by such organic light emitters, the road towards spectrally broad white light polymer emitters still holds many design challenges.

Enhancement methods for efficient light emission have been studied for several inorganic semiconductors, and one very effective approach to developing highly efficient light emitters has been based on the incorporation of metals for the efficient extraction of light. Recently, we reported dramatic enhancements of the light emission from inorganic<sup>1,2</sup> and organic<sup>3</sup> light emitters using surface plasmon coupling. These can now be applied towards OLED material and incorporated together with advances in polymer chemistry that have recently resulted from the addition of fluorine-based polymers or phosphors.<sup>4,5</sup>

## Experiment

Here we focus on increasing the light-emission efficiency from optimized blue light-emitting polymers through the use of surface plasmons for enhancement of the internal quantum efficiency. Three conjugated polymers were studied: PF-CNP (1:1), PF-CNP (3:1), and PF-TPA-Q. The molecular structures for the conjugated polymers used are illustrated in Figure 1.<sup>7,8</sup> The corresponding conjugated polymers PF-CNP (1:1), PF-CNP (3:1), and PF-TPA-Q will be referred to as pf1cnp1, pf3cnp1, and pftpaq, respectively. The conjugated polymers were dissolved in chlorobenzene to form a 2%

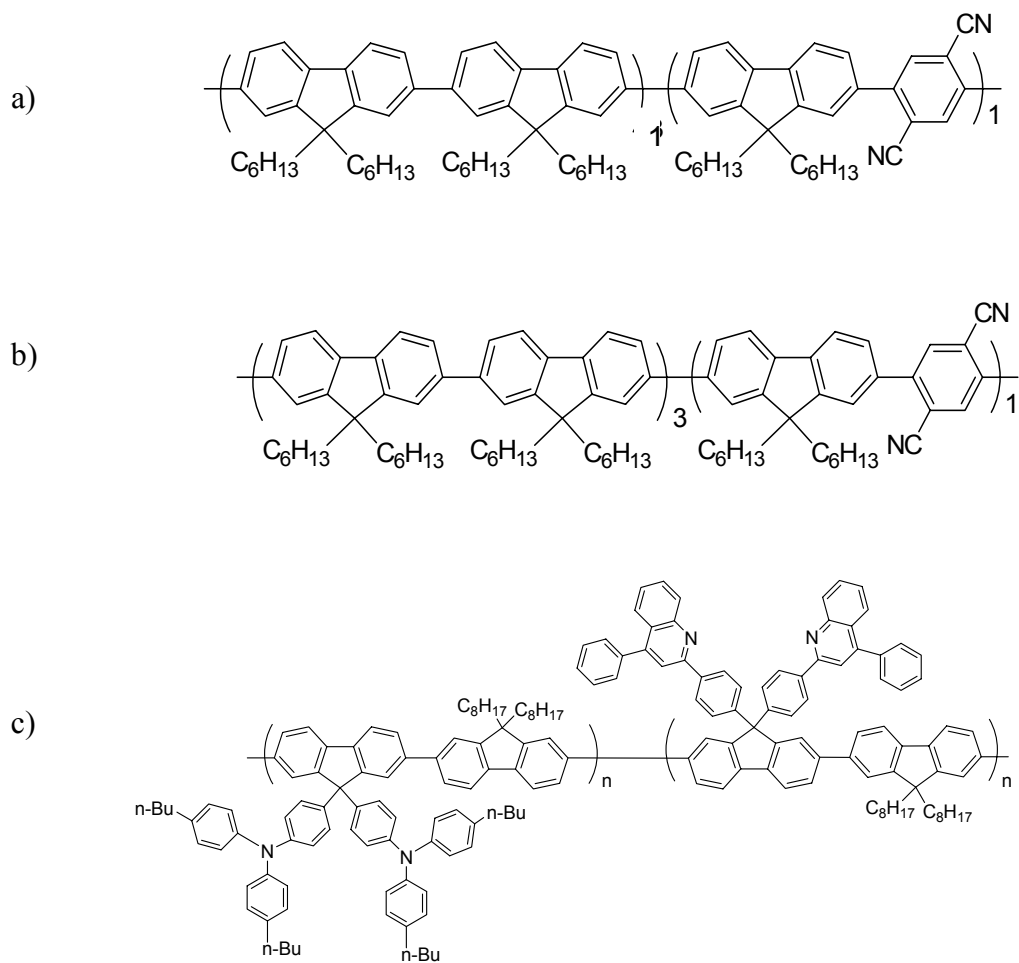


Figure 1 Molecular structures for (a) pf1cnp1,<sup>7</sup> (b) pf3cnp1,<sup>7</sup> (c) and pftpaq.<sup>8</sup>

(by volume) solution. This solution was then spun onto a quartz sample, half of which had previously been coated with a 50 nm silver layer. Photoluminescence measurements were then performed to compare the different areas of the sample, comparing the luminescence efficiency from emitters with no metal with those in proximity to the metal.

Similar to Chapter 3,<sup>3</sup> the sample geometry consists of quartz samples covered with silver and light emitting polymer layers. In this Chapter, however, conjugated polymers are used instead of a dye-doped polymer films, and we present new photoluminescence results on these much more efficient emitter materials, in which the fluorophore concentration is higher compared to laser dyes doped within a polymer matrix. More interesting observations are possible with such efficient polymer emitters.

The experimental setup and measurements for detecting emission intensity enhancements is described in our previous work<sup>3</sup> on enhanced emission from dye-doped polymer layers. An InGaN 405 nm diode laser was used to excite the samples. A Princeton Instruments Cooled CCD and Acton Research Corporation Spectrograph were used to perform measurements of the emission intensities of these samples. Moreover, a Hamamatsu Photonics streak camera was used to obtain time-resolved photoluminescence (TRPL) spectroscopy data from polyfluorene emission rates after deposition on silver coated quartz samples. For the TRPL measurements, a frequency doubled beam of a mode-locked Ti sapphire laser (Spectra Physics) was used to excite the samples. The pulse width, wavelength, and repetition rate were chosen as 100 fs, 400 nm, and 80 MHz, respectively. These TRPL studies determined decay rates at various wavelengths, as well as the Purcell<sup>6</sup> factors. Carrier dynamic measurements were observed to be correlated with measured photoluminescence intensity enhancement ratios,

and confirm that some conjugate polymers are better suited for luminescence enhancement resulting from coupling to surface plasmons. A neutral density filter was added in the setup just before the detector as the signal intensities were significantly larger than from our previous dye-doped polymer work. By employing the use of a shutter, photo-oxidation of these somewhat unstable conjugated polymers could be largely avoided.

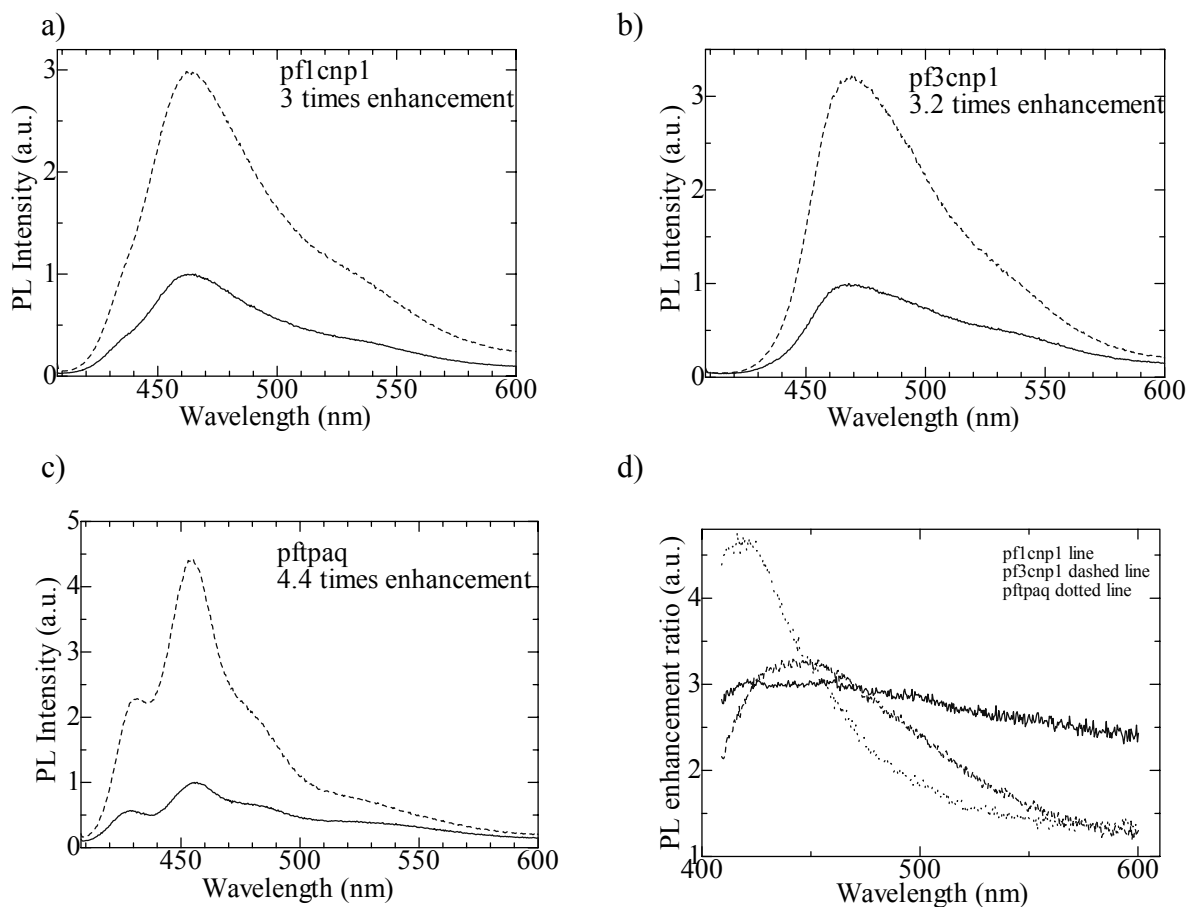


Figure 2 PL enhancements, (a) pf1cnp1, (b) pf3cnp1, (c) pftpaq and (d) enhancement ratios plotted against the wavelength.

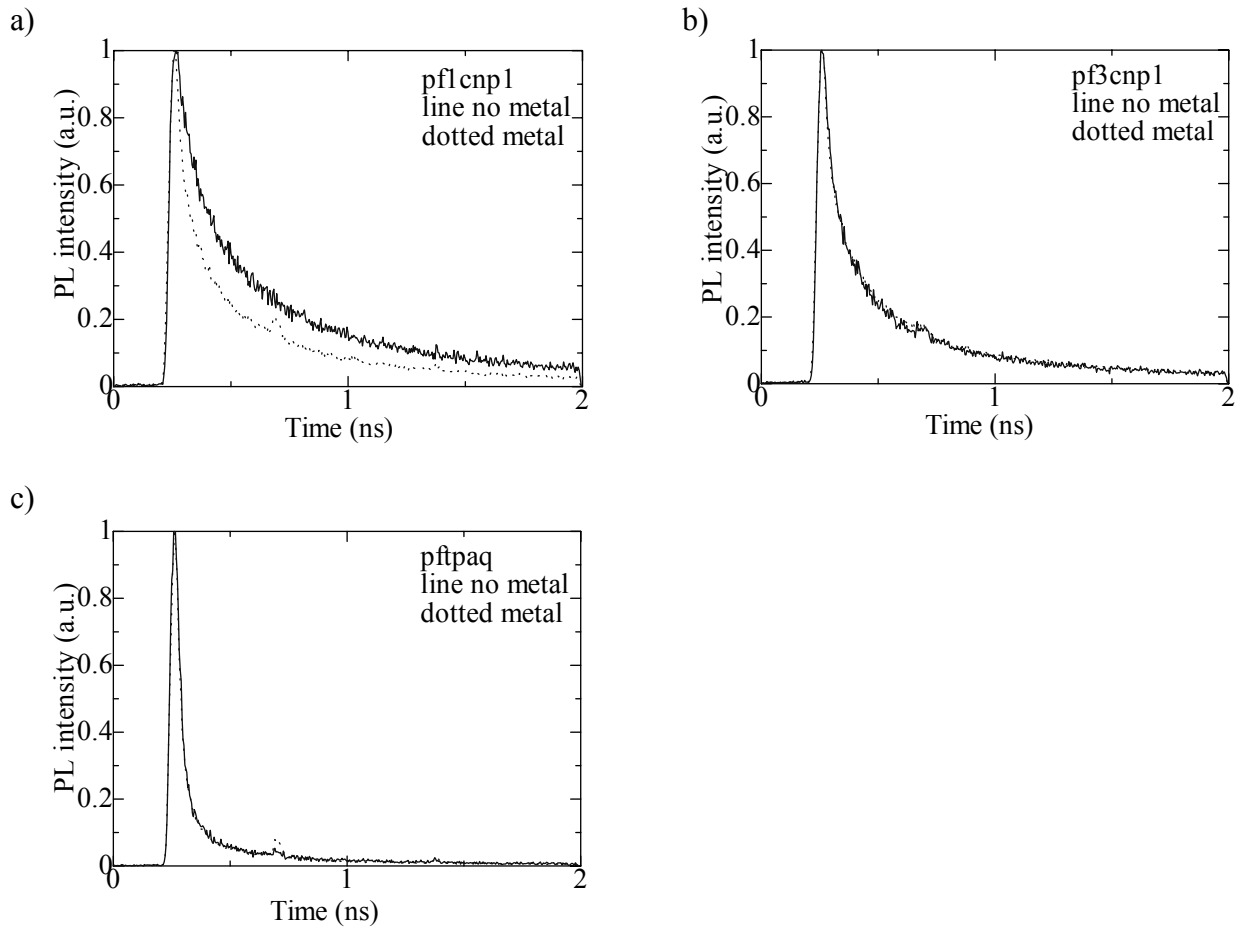


Figure 3 TRPL with the data normalized to 1 where the dotted line shows the conjugated polymer carrier decay rate with metal and solid line without metal, (a) pflcnp1, (b) pf3cnp1, (c) pftpaq.

## Results and Discussion

The enhancements observed for pf1cnp1, pf3cnp1, pftpaq, were 3, 3.2, and 4.4 times, respectively, and are shown in Figures 2a–c. In Figure 2d the enhancement ratios for each conjugated polymer reflect a maximum enhancement for shorter wavelengths. A larger contribution due to the surface plasmon coupling is evident, as shorter wavelengths have higher enhancements. This finding can be explained by the surface plasmon dispersion diagram, which indicates a better match between the silver plasmon resonance and the emission at shorter wavelengths.<sup>3</sup>

Figure 3 compares the time-resolved PL decay profiles between the conjugated polymers deposited on quartz and on silver films on quartz sample. Longer PL lifetimes were measured for the conjugated polymer on bare quartz. The observation of a faster decay profile for pf1cnp1 on metal on quartz suggested that there was significant transfer of energy between the conjugated polymer and the silver surface plasmon polariton. Conjugated polymers with bipolar charge-transporting properties, namely pf3cnp1 and pftpaq, already exhibited fast decay rates without the silver layers and therefore the lifetime is similar to that when surface plasmons are coupled, in turn providing no significant reduction in the PL lifetime,  $\tau_{PL}$ . However, for the better electron transporter pf1cnp1, energy transfer is facilitated to the surface plasmons and results in shorter PL lifetimes.

The internal quantum efficiency,  $\eta_{int}$ , is described as the radiative recombination rate divided by the sum of the radiative,  $k_{rad}$ , and nonradiative recombination rates,  $k_{nonrad}$ , as shown below.

$$\eta_{\text{int}} = \frac{k_{\text{rad}}}{k_{\text{rad}} + k_{\text{nonrad}}}$$

where the PL lifetime is the inverse of the recombination rate, (i.e.,  $\frac{1}{\tau_{\text{PL}}} = k_{\text{rad}} + k_{\text{nonrad}}$ ).

For the surface plasmon case, the enhanced efficiency,  $\eta_{\text{int}}^*$ , is better described by the sum of the recombination rates that are radiative and due to surface plasmons,  $k_{\text{sp}}$ , divided by the sum of the radiative, nonradiative, and surface plasmon recombination rates, as listed below.<sup>1,2</sup>

$$\eta_{\text{int}}^* = \frac{k_{\text{rad}} + k_{\text{sp}}}{k_{\text{rad}} + k_{\text{nonrad}} + k_{\text{sp}}}$$

If initially the efficiency is high, the influence from the surface plasmons is not significant. The coupling due to surface plasmons can become very significant when the initial quantum efficiency is low.

In Figures 4a–c, the photoluminescence lifetimes are plotted versus the emission wavelengths. Carrier lifetimes are shorter for the case when the conjugated polymer was deposited on the metal films. In Figure 4d, we also plot the calculated Purcell factors versus emission wavelengths for the three conjugated polymers. These Purcell factors represent the average of several measurements taken for each conjugated polymer. Again, the pflcnp1 sample showed the greatest influence on the metal surface. When the initial lifetime was short, coupling into surface plasmons did not significantly decrease the lifetime. For the case when the initial lifetime was long, however, surface plasmons could substantially decrease the lifetime and increase the quantum efficiency.

Taking an in-depth look at the properties of the polyfluorenes studied can reveal the mechanisms that offer themselves to better coupling potential. A high efficiency due

to better charge injection and more efficient charge recombination was reported by Shu for PF-TPA-Q.<sup>8</sup> Liu et al. extensively studied such properties of the PF-CNP (3:1) and

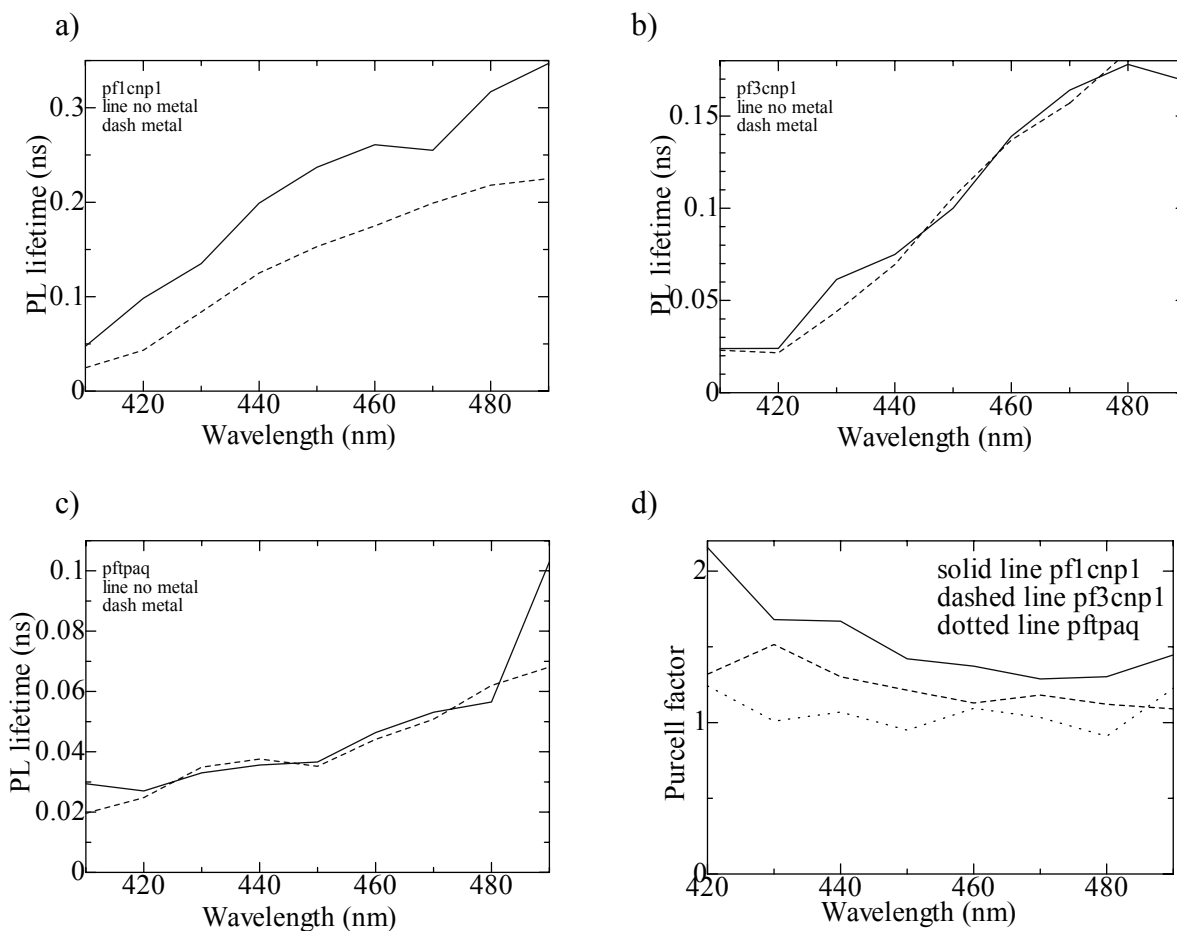


Figure 4 Carrier lifetime plotted against the wavelength (a) pf1cnp1, (b) pf3cnp1, and (c) pftpaq. Average Purcell factor for the conjugated polymers studied.

PF-CNP (1:1), where the solid state PL efficiencies were reported as 66% and 48%, respectively.<sup>7</sup> They also attributed the slow electron motion to the higher content of cyano constituents that stabilize the radical anion and to the less planar structure of PF-CNP (1:1). For these reasons, we expect the surface plasmon polaritons to assist in the movement of these electrons, coupling enough energy to increase electron transport. Some enhancement due to the coupling of surface plasmons was evident in the PL data obtained from the metal side. These enhancements, however, were not as significant as for the dye-doped polymer layers. We attribute this observation to the notion that the efficiencies of the conjugated polymers are already high and we expect the coupling due to surface plasmons to have a smaller effect on the enhancement in this case.

## **Conclusion**

From studying the TRPL of these polyfluorenes in conjunction with the PL enhancement ratios we have found that those with longer carrier lifetimes offer large improvements in quantum efficiency if surface plasmons are used to enhance recombination of electron-hole pairs. Although only 3 or 4 times emission enhancements are observed this is a significant increase in quantum efficiency from these state-of-the-art organic light emitters. We expect that, along with the development of robust and efficient polymers, the use of surface plasmons will ultimately lead to highly efficient polymer light emitters that can be used for solid state lighting applications.

**References**

- <sup>1</sup>K. Okamoto, I. Niki, A. Scherer, Y. Narukawa, T. Mukai, and Y. Kawakami, *Applied Physics Letters*, 87, 071102, 2005.
- <sup>2</sup>K. Okamoto, I. Niki, A. Shvartser, Y. Narukawa, T. Mukai, and A. Scherer, *Nat. Mater.* 3, 601, 2004.
- <sup>3</sup>T. D. Neal, K. Okamoto, and A. Scherer, *Optics Express* 13, 14, 5522–5527, 2005.
- <sup>4</sup>F. Hide, P. Kozodoy, S. P. DenBaars, and A. J. Heeger, *Appl Phys. Lett.* 70, 20, 1997.
- <sup>5</sup>C. Zhang and A. J. Heeger, *Journal of Appl. Phys.*, 84, 3, 1998.
- <sup>6</sup>E. M. Purcell, *Phys. Rev.* 69, 681, 1946.
- <sup>7</sup>M. S. Liu, X. Jiang, P. Herguth, and A. K-Y. Jen, *Chem. Mater.*, 13, 3820–3822, 2001.
- <sup>8</sup>C-F. Shu, R. Dodda, F-I. Wu, M. S. Liu, and A. K-Y. Jen, *Macromolecules*, 36, 6698–6703, 2003.

## **Unifying summary**

A great deal of interest during my thesis work came from nanotechnology in many areas. Some areas related to microfluidics and others to nanophotonics. The general underlying theme was that nanofabrication tools were used and the idea of miniaturizing things and taking advantage of the physics involved brought all of this work together. Light manipulation remained a common thread in the majority of the work included in this thesis.

## **Chapter 5–Nanofabricated devices and applications**

This chapter covers several devices focusing on their fabrication methods.

## **Metal nanostructures on insulator**

There has been some interest in fabricated structures on insulating materials, especially when the desire is to have a substrate that does not interfere with electrical measurement and when a thin insulating layer on the substrate is not enough. With UV lithography, structures a few microns in size and a little smaller are possible. However, when wanting to get sub-micron features, one would have to turn to electron beam lithography and then find it somewhat challenging since the insulator does not conduct and is not allowed to dissipate the charges thereby having a state of charging up on the surface. Therefore researchers turned to imprint lithography. The technology nano-imprint<sup>1-2</sup> lithography has been demonstrated for grating-type structures where the geometry is on the order of tens of nanometers, but requires an electron beam written mold.

Here experimental results are presented on nanostructures fabricated on insulating materials with a method that will allow complex structures to be made without using a mold but instead using mask layers. The device proposed, not to be described but only mentioned, is an electromagnetic trap.

## **Experimental procedures**

In this procedure we used a fused quartz slide and prepared it with a sacrificial layer by applying 130 nm of polymethylmethacrylate (PMMA) and baking it for 20 minutes at 180° C. Since sub-micron patterns were desired on an insulating substrate we applied a 100 nm Au film by thermal evaporation to prevent charging on the surface during electron beam lithography. Several samples with different thickness of Au film were

used to figure out the optimum thickness. In searching for an optimum thickness, the chosen dose level with a 100 kV beam would yield a nice pattern with a 100 nm Au film, which provided sufficient material for conductivity. Then PMMA was again applied this time as the layer for electron beam writing with the same specification as above. The Lieca EBPG was used to obtain the 100 kV beam for electron beam writing. Upon developing of a 30 kV converted SEM beam-written pattern, the following image was obtained, shown as Fig 1a.

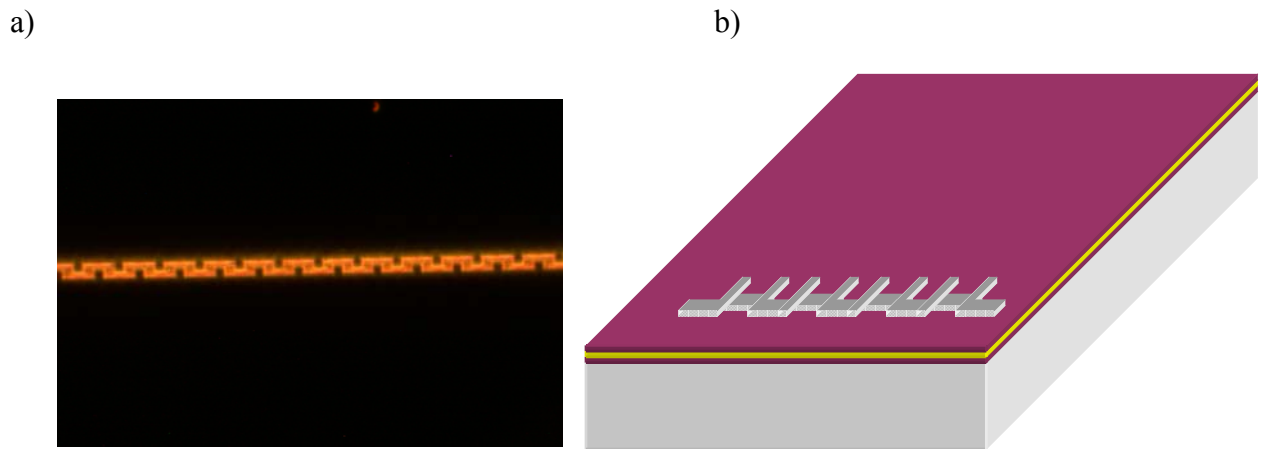


Figure 1 a) Corrugated pattern in PMMA, on Au, on PMMA, on quartz. b) Cartoon of layered structure, where the middle layer is the sandwiched Au between PMMA layers, and an example pattern are shown.

Calibration beam-written samples were done first using silicon and silicon on insulator samples. The fabrication steps for those samples are shown in Figure 2.

However, the goal consisted of fabricating structures on quartz.

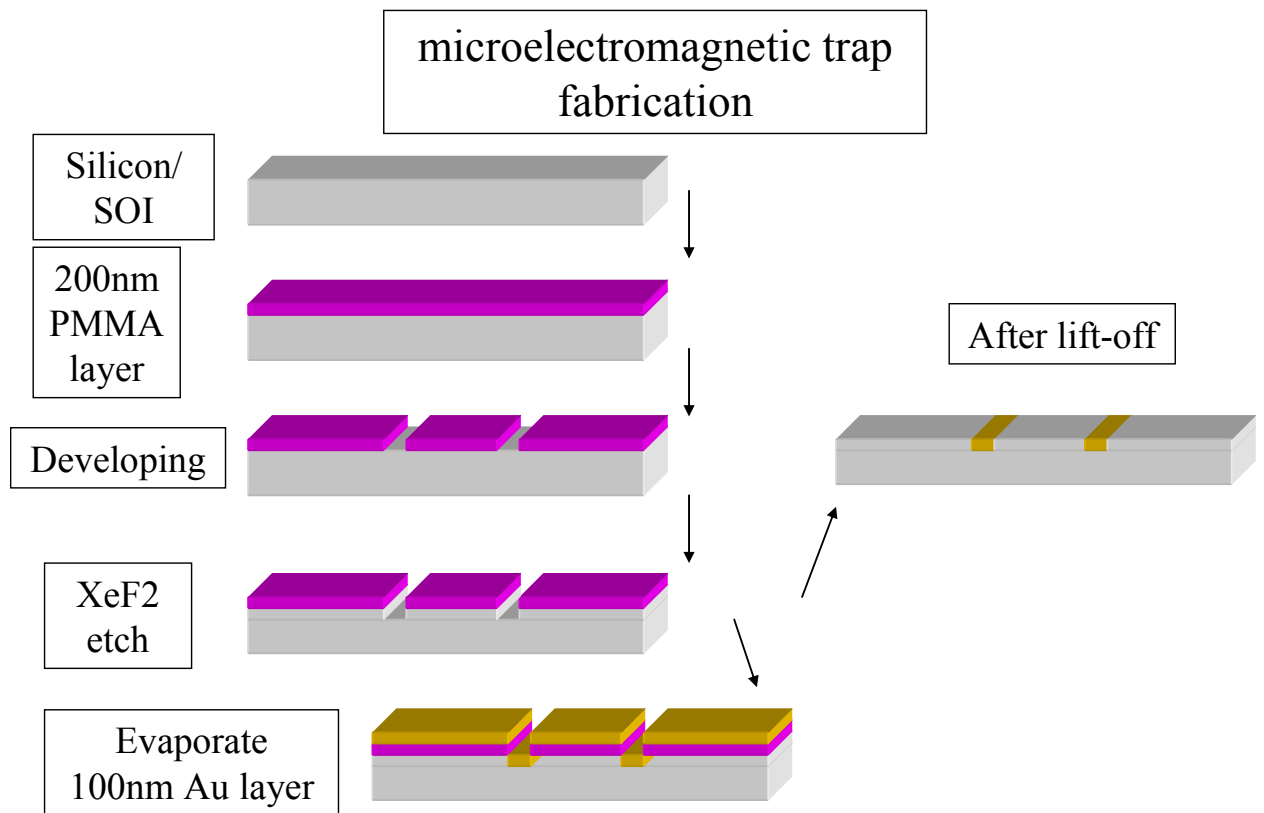


Figure 2 Fabrication steps to obtain metal filled trenches within a sample.

Next a series of etching techniques were undertaken. For pattern transfer, an argon plasma was used to mill through the 100 nm of Au, using the top layer of PMMA as a mask. Given that the desire was to etch the underlying quartz, the bottom layer of PMMA in the patterned region had to be removed before the SiO<sub>2</sub> etch. By using oxygen and argon plasma this challenge was accomplished for the 130 nm PMMA film. The etch gas of choice was CHF<sub>3</sub> considering the etch rate associated with it for quartz.

Following this procedure, the etched pattern was filled with gold, and what remained of the Au sandwiched within PMMA layers was removed with acetone as shown in Fig 3.

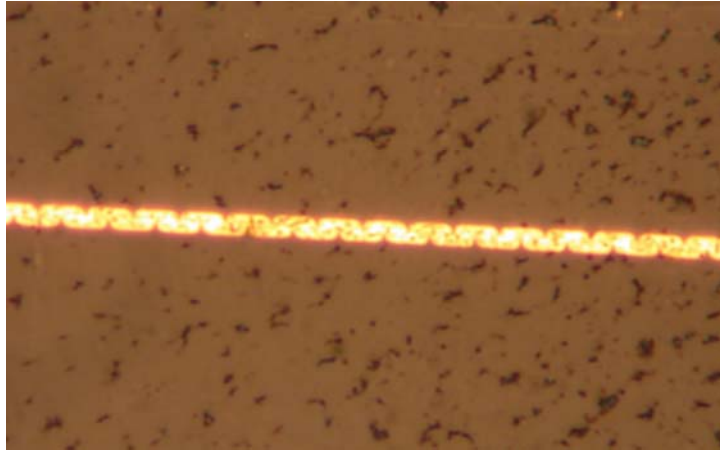


Figure 3 Optical microscope image of gold-filled corrugated trench in quartz.

### **Results and discussion**

In the initial stages of this work, a scratch on the substrate was used to go from the macro world to the microelectromagnetic trap. This scratch would remove PMMA such that when evaporation was done the metal filling the void would be large enough for aligning a probe tip for electrical contact. Otherwise, another optimal way to accomplish contact would have been to add a UV lithography step after the first lift-off to align contact pads. The use of the EBPG, electron beam pattern generator, allowed for lithographically defining the small trap structures while also making the contact pads sufficiently large enough, preventing an extra lithography step, Figures 4–7.

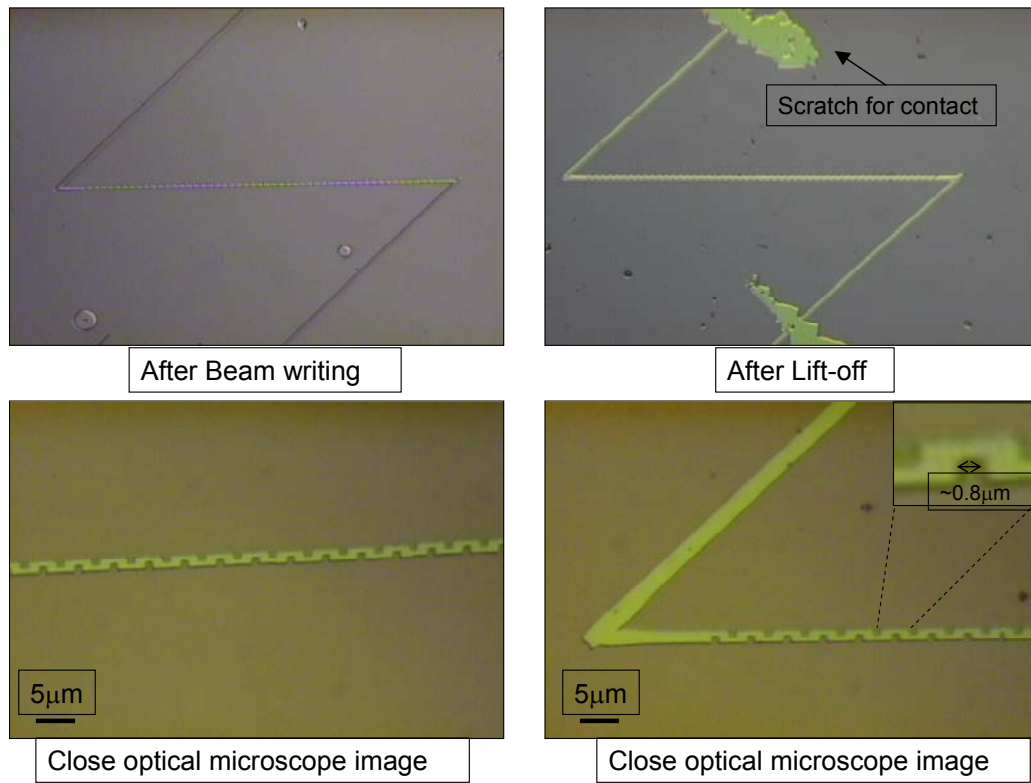


Figure 4 Corrugated wire structures at various stages of fabrication.

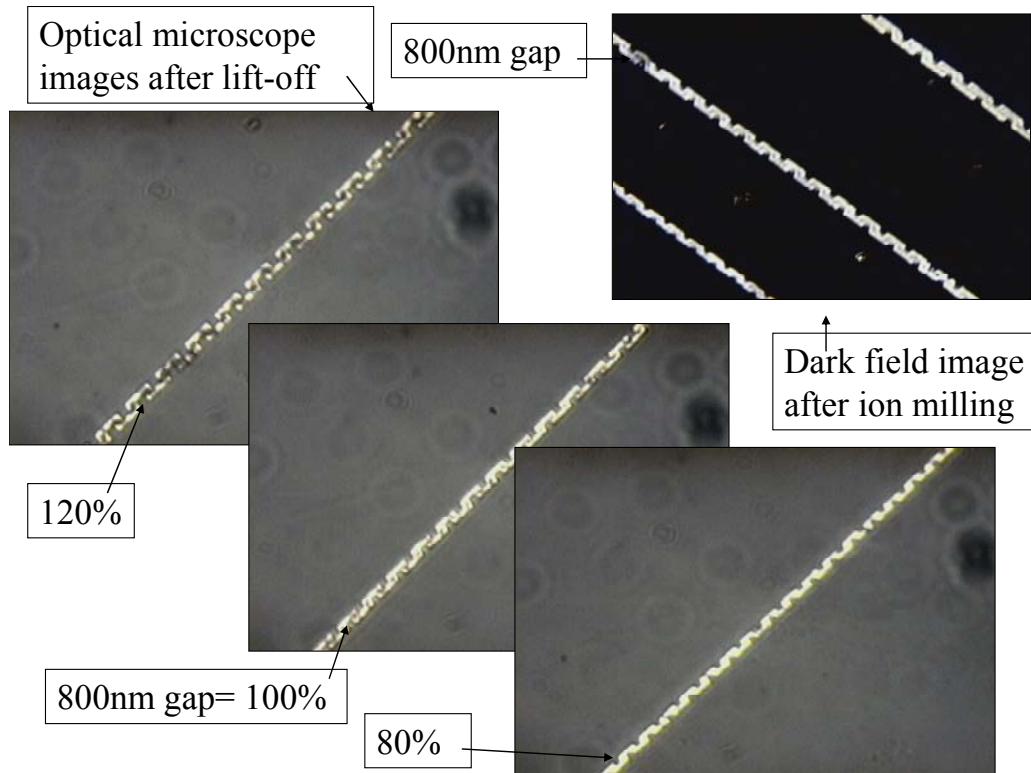


Figure 5 Images showing the quality of the structures.

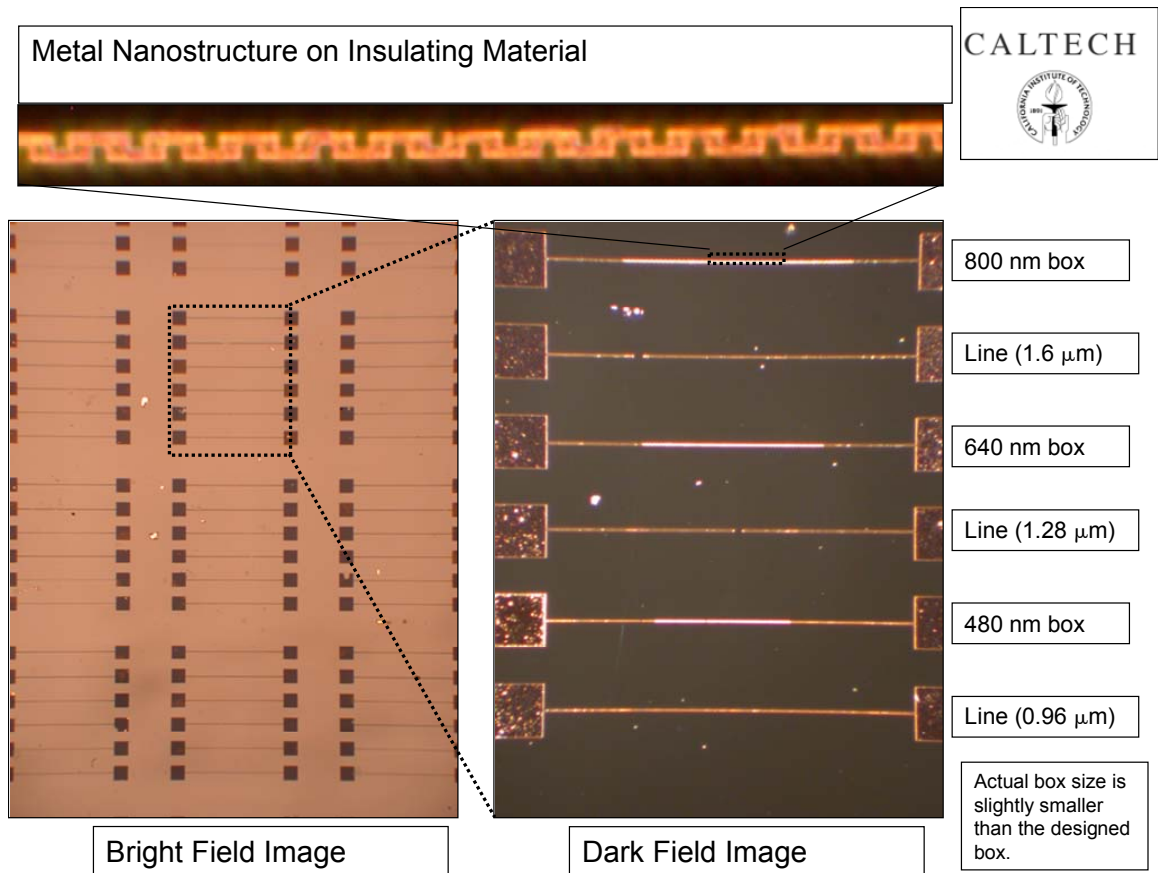


Figure 6 Images of arrays of electron beam-written patterns of different specifications.

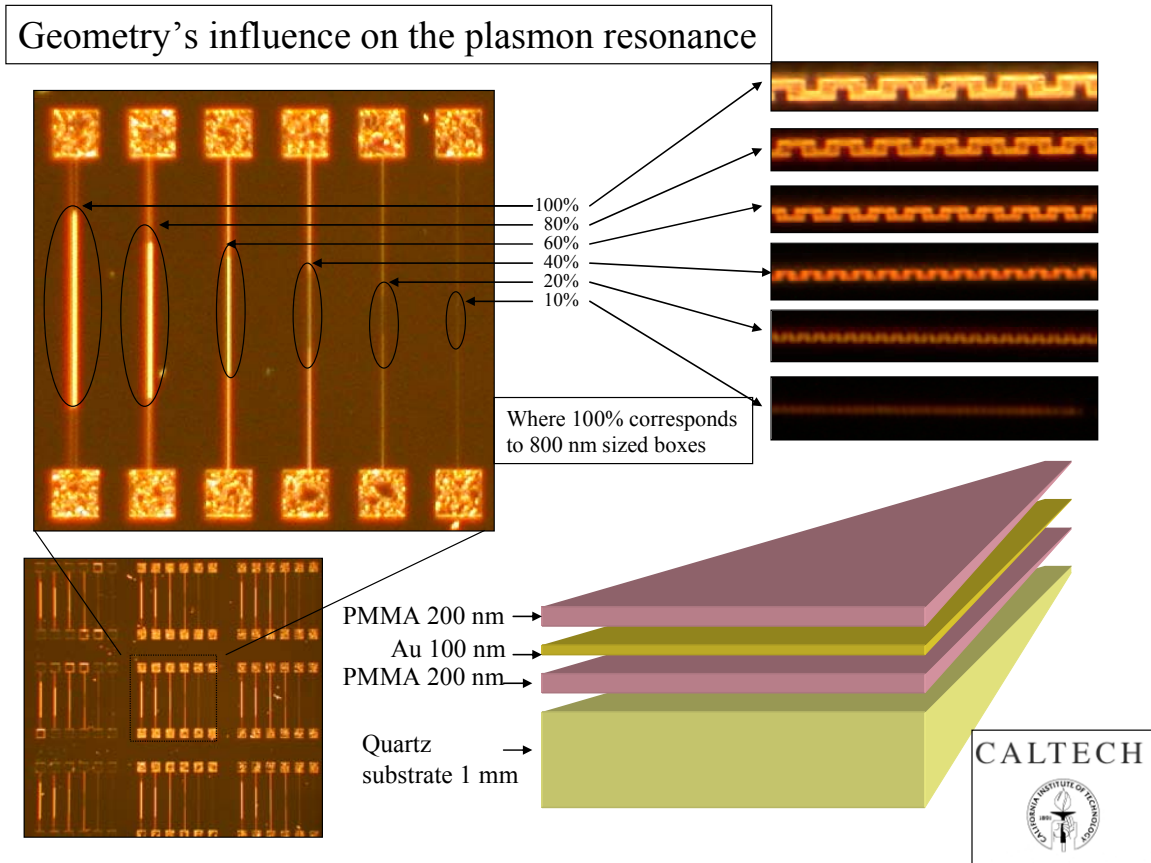


Figure 7 Images of gold corrugated lines with contact pads and cartoon of structure.

## DNA Conductivity

In this project we seek to perform a direct measurement of DNA's conductivity in solution. Several samples with evenly distributed gold pads were fabricated for analysis purposes. One convention was using an array of circles of 100 nm spaced by 5  $\mu\text{m}$ . Another convention was using sub-100nm lines spaced by 100 nm.

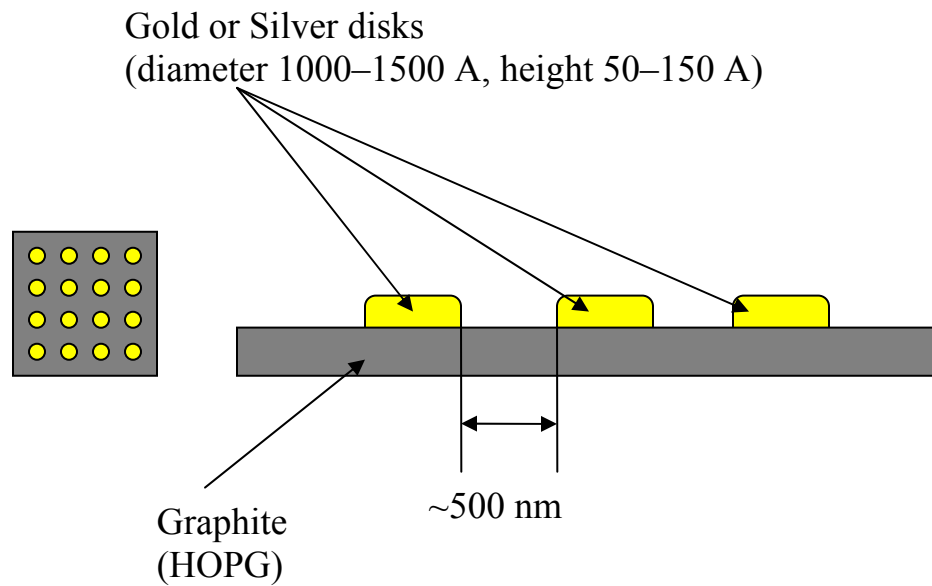
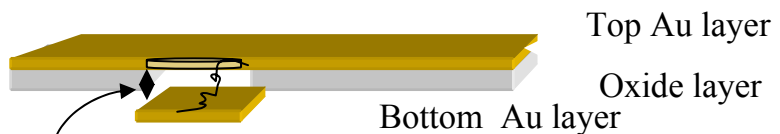
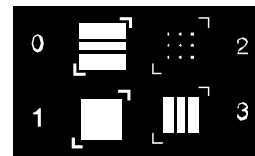


Figure 8 Proposed isolated gold mounds on graphite sample schematic.

- Layer 0 Au pattern
- Layer 1 oxide pattern
- Layer 2 etch pattern
- Layer 3 Au pattern



Defining thickness

Figure 9 Mask design for making the structure and schematic of structure.

### Nanostructured insulator for metal nanoparticle analysis device

The goal of this project involved making a device for nanoparticle analysis. Silver nanoparticles around 10 nm in size and less were coated with a polymer shell with the intention of aligning them on a substrate such that they could be placed in a single row. Advantages one would obtain from using the small particles would be 1) the particles, with their small size, could be easily combined with other existing devices, 2) in solution the particles could be easily spun onto a substrate, and (one of the main reasons) 3) the electromagnetic field of such small particles exceeds the diameter of the particle, which lends itself to near field interaction.

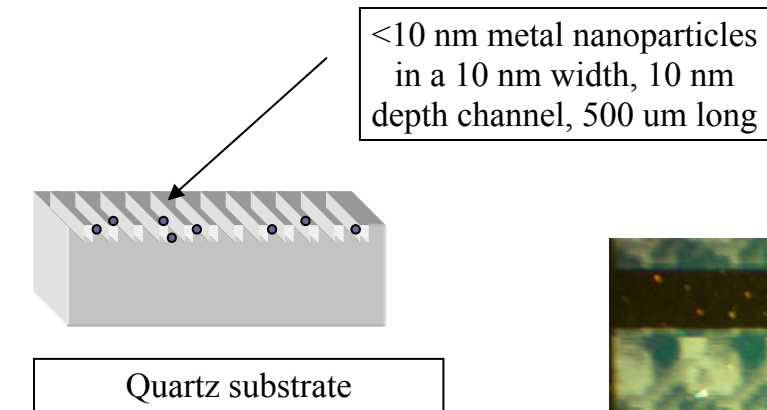


Figure 10 Schematic of nanostructure sample.

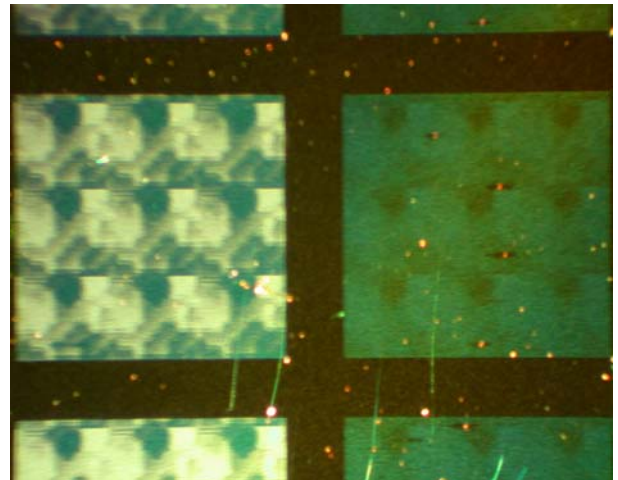


Figure 11 Optical microscope image of channels in metal on quartz.

**Conclusion**

Sub-100 nm structures were fabricated in an insulating material without the use of nano-imprint lithography simply by using a combination of metal and polymer sacrificial layers. Further studies will make use of these structures for analysis of nanoparticles or sensing applications.

**References**

- 1 M. D. Austin, S. Y. Chou, Appl. Phys. Lett. 81, 4431 (2002)
- 2 H. Cao, Z. Yu, J. Wang, J. O. Tegenfeldt, R. H. Austin, E. Chen, W. Wu, W. Y. Chou, Appl. Phys. Lett. 81, 174 (2002)

## **Chapter 6–Molecular dynamics study of photochromic molecules probed by the mask pattern transferred-transient grating technique**

### **Abstract**

Mask pattern transferred-transient grating (MPT-TG), which is a convenient new technique in the class of optical heterodyne detected-transient grating (OHD-TG), is applied to photochromic molecule (spiropyran) in 2-propanol solution. The spatial modulation of optical properties of the material is generated by transferring an ultra-violet light pattern directly from a metal film grating into the sample solution and detected through the diffraction of a probe beam. The thermal conductivity of the solvent and the diffusion coefficients of the solute molecules were obtained and compared with the calculated values. This method has many advantages compared to the conventional techniques.

## Introduction

The transient grating (TG) technique, which is one of the third order nonlinear spectroscopies, has been a useful and powerful tool for studies in photonics and in photochemical processes of solutions.<sup>1-6</sup> This technique has many unique advantages. For example, it is capable of monitoring molecular dynamics of short-lived chemical species in solutions.<sup>7-10</sup> However, there are several difficulties in this technique. The diffracted signal intensity ( $I_{TG}$ ) is given by the sum of the square of refractive index change ( $\delta n$ ; phase grating) and absorbance change ( $\delta k$ ; amplitude grating) induced by the optical interference pattern. The quadratic nature of the signal intensity makes the analysis of the signal components complicated. Also, contributions of the phase and amplitude gratings are difficult to separate from each other. Another difficulty of this technique is its weak signal intensities, so that a highly sensitive optical detection technique is required.

In order to improve these difficulties, the optical heterodyne detected-transient grating (OHD-TG) has been devised.<sup>11-12</sup> In this technique, a local oscillator field is mixed coherently with a signal field on a detector. The local oscillator enhances the signal intensities up to a factor of 100, and  $\delta n$  and  $\delta k$  can be separated by controlling the phase difference ( $\Delta\phi$ ) between the local oscillator and the signal. Moreover, it has a linear relationship between the signal intensity and  $\delta n$  (or  $\delta k$ ). However, the experimental setup of the OHD-TG is more complicated and difficult. A primary difficulty is to keep the phase stability between the local oscillator and the probe beam. A new simple OHD-TG setting has been reported<sup>13-16</sup> using an optical diffractive element to achieve sufficient phase stability. Terazima<sup>17-18</sup> reported the much improved and simple setting of the OHD-

TG by using a tilt angle controlled neutral density filter to control the relative  $\Delta\phi$  by changing the light path length. Katayama et al.<sup>19-21</sup> developed a lens-free OHD-TG technique by using a transmission grating structure in a 3 mm glass.

Recently, we have reported<sup>22</sup> the mask pattern transferred-transient grating (MPT-TG) technique, which is a convenient new technique of the OHD-TG class with a metal film grating fabricated in our laboratory. We also showed that this technique is well applicable for highly sensitive molecular detection for microfluidic devices.<sup>23</sup> In this paper, this technique is applied to study the chemical reaction and molecular dynamics of photochromic molecule (spiropyran) in 2-propanol solution.

## Method

Fig. 1a shows the pump and probe beam alignments for a typical OHD-TG technique. Two pump beams (intensity:  $I_e$ , wavelength:  $\lambda_e$ ) are crossed with angle ( $\theta_e$ ) to make an optical interference pattern (optical grating,  $\delta I$ ) at the sample. The fringe spacing ( $\Lambda$ ) of the optical grating is given by  $\Lambda = \lambda_e / 2 \sin \theta_e$ . After that,  $\delta n$  and  $\delta k$  of the solution are also modulated along the optical grating. Both modulated  $\delta n$  and  $\delta k$  behave as diffraction gratings and can be detected by the first-order diffracted beam of the probe beam (intensity:  $I_p$ , wavelength:  $\lambda_p$ ). In order to enhance the diffracted signal intensity ( $I_s$ ), the signal is superimposed to the reference beam ( $I_r$ ), which provides a local oscillation field. As shown in Fig. 1a, four laser beams (two pump beams, a probe beam, and a reference beam) must be tuned one by one in order to focus at the same spot in the sample. Two pump beams must be controlled by an optical delay to maintain coherence. Thus the optical alignment of this technique is very complicated and difficult. Moreover, probe

beam and reference beam must be tuned to keep  $\Delta\phi$  stable. These tunings are tedious and unstable.

In contrast, Fig. 1b shows a schematic diagram of MPT-TG technique, which is

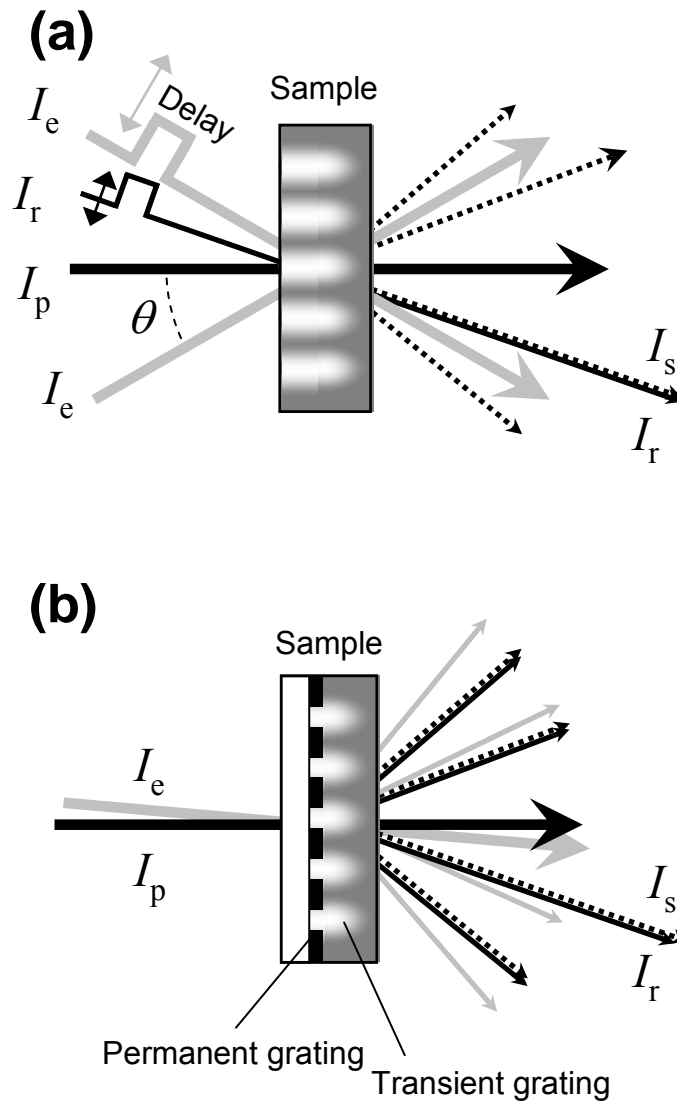


Fig. 1. Pump and probe beams alignments for (a) traditional optical heterodyne detected-transient grating (OHD-TG) technique and (b) the present mask pattern transferred-transient grating (MPT-TG) technique.

made both simple and stable by inserting a metal grating, eliminating one of the pump beams and the redundant  $I_r$  input.

The tunings of delays or angles of these beams are not required, while the MPG-TG has the same advantage of the usual OHD-TG.. The grating pattern is thus transferred from the metal film to the sample solution such that a similar optical grating is created. More details of the pattern transfer are shown in Fig. 2. At the bright region, many molecules are excited and chemical products are generated by this photochemical reaction. Therefore, molecular concentrations of chemical products are also spatially modulated (concentration grating,  $\delta C$ ). Temperature in solution is also spatially modulated (thermal grating,  $\delta T$ ) by the energy released through nonradiative relaxation from the excited molecules. Both  $\delta C$  and  $\delta T$  contribute to induced  $\delta n$  and  $\delta k$ . A further simplicity of this optical setting is that two types of the diffracted patterns are generated from the probe beams, namely, diffraction from the metal grating and that from the transient grating. The former is an invariant diffracted light whereas the latter is variable since all  $\delta C$ ,  $\delta T$ ,  $\delta n$ , and  $\delta k$  are functions with time ( $t$ ) and space ( $x$ ). The invariant beam acts as a reference beam ( $I_r$ ) to provide a local oscillation field and enhances the variable signal beam ( $I_s$ ) by orders of magnitude. The conditions required for heterodyne detection are automatically satisfied, since both beams have completely the same originality, position and direction. In this setup,  $\Delta\phi$  is decided only by the thickness of the metal grating. Therefore, the phase stability of this setup is excellent contrasted to the tuning difficulty and the unstable  $\Delta\phi$  that characterize the usual OHD-TG.

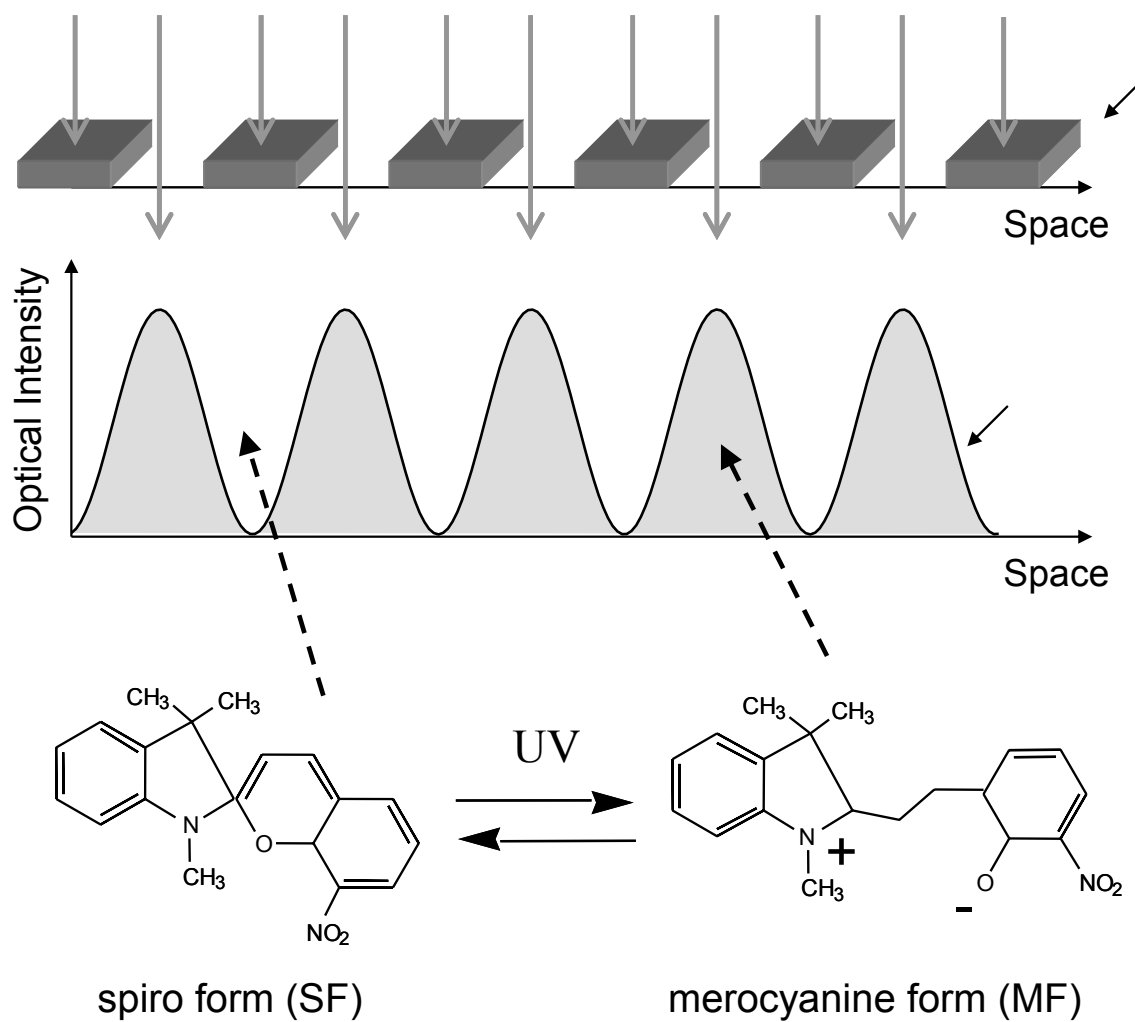


Fig. 2. Schematic diagram of the permanent metal grating and induced spatial modulation of light intensity. Spiropyran molecules were photoexcited and transformed from merocyanine form (MF) to spiropyran form (SF) along the bright-dark pattern.

## Experimental

The experimental setup of the MGT-TG has already been published elsewhere.<sup>22,23</sup> A frequency-tripled Nd:YAG laser ( $\lambda_e = 366$  nm,  $I_e = 0.3$  mJ/pulse) and a cw-He-Ne laser ( $\lambda_p = 633$  nm,  $I_p = 0.05$  mW) are used as the pump and the probe beams, respectively. The pulse width and repetition rate of pump beam are 10 ns and 10 Hz, respectively. Both pump and probe beams are focused by a lens on the sample solution. The pump beam is not tightly focused (spot size  $\sim 1$  mm) on the sample to avoid any multiphoton process, higher-order reaction, or transient lens contribution.<sup>17-18</sup> Two types of diffracted signal  $I_r$  and  $I_s$  are isolated from the pump beam with a pinhole and a glass filter and detected with an InGaAs photodetector. Time profiles of the signals were measured with a 100 Hz digital oscilloscope.

To make a metal grating, a chromium layer (100 nm) was deposited by the vacuum evaporation on the quartz substrate. A fine grade photo resist was deposited on a Cr layer by spin coating. Micrometer-scaled patterns were written by the lithography of a direct writing laser. Finally, metal grating structures were engraved by chemical etching. The grating period is  $\Lambda = 9$   $\mu\text{m}$ .

The sample solution used is spiroiran [1', 3', 3'-trimethyl-8-nitrospiro (2H-1-benzopyran-2, 2'-indoline)] in 2-propanol. The concentration is about 5 mM. The photochemical reaction scheme of this molecule is shown in the bottom row of Fig. 2. The excited molecules produce colored isomer (merocyanine form; MF) while the ground state (spiro form, SF) is transparent at the probe wavelength. That is the reason why this molecule is called a photochromic molecule. The spiroiran (Eastman Kodak) was purified by recrystallization. Spectroscopic grade solvent 2-propanol is used as received.

## Results and Discussion

Fig. 3 showed the time profiles of the TG signals in microsecond time scale (a) and millisecond timescale (b). The dashed line in each figure is the signal intensity of the reference beam ( $I_r$ ). After excitation, the diffracted beam intensity rose rapidly and decayed with microsecond timescale. The signal decayed lower than baseline ( $t=0$ ). This negative signal component decays on a millisecond timescale and tends to the baseline finally. The total signal intensity ( $I_{total}$ ) is given by<sup>12,15-19</sup>

$$I_{total}(t) = I_r + 2a[\chi^{(3)'}(t)\cos\Delta\phi + \chi^{(3)''}(t)\sin\Delta\phi]I_e I_p + |\chi^{(3)}(t)|^2 I_e^2 I_p \quad (1)$$

where  $\chi^{(3)'}(t)$  and  $\chi^{(3)''}(t)$  are the real part and imaginary parts, respectively, of the third order nonlinear electrical susceptibility  $\chi^{(3)}(t)$ , and  $a$  is a real constant. The third term indicates the TG signal with usual homodyne detection and is negligible because  $\chi^{(3)}$  in solution should be very small. Thus, only the second term of Eq. (1) indicates  $I_s$ , and this provides a large enhancement of the signal intensity and a linear relationship between the output signal and  $\chi^{(3)}$ . The obtained time-variable signal is the TG signal ( $I_{TG}(t)$ ) corresponding to the second term of Eq (1). In this case,  $\chi^{(3)'}(t)$  and  $\chi^{(3)''}(t)$  are equal to  $\delta n(t)$  and  $\delta k(t)$  induced by the transient grating, respectively. Thus, the second term of Eq. (1) can be written as

$$I_{TG}(t) \cong \delta n(t)\cos\Delta\phi + \Delta\delta k(t)\sin\Delta\phi \quad (2)$$

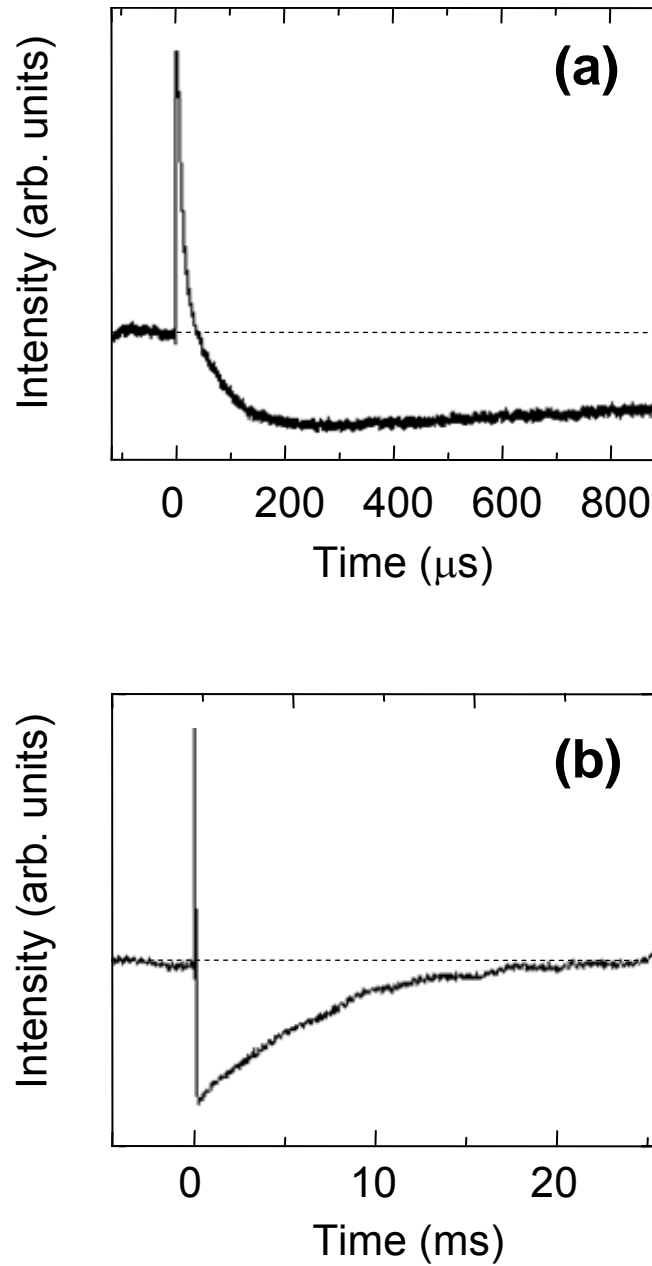


Fig. 3. Time profiles of the diffracted signals (TG signals) in microsecond timescale (a) and millisecond timescale (b). The dashed lines denote the initial intensities of the reference beam ( $I_r$ ).

The origin of the fast decayed positive signal and the slow decayed negative signal observed in Fig. 3 should be different. As mentioned above, the thermal grating ( $\delta T$ ) and concentration grating ( $\delta C$ ) can contribute to the signal time-profile. These contributions are given by the following relationships:<sup>9</sup>

$$\delta n = \left[ \left( \frac{\partial n}{\partial \rho} \right)_T \frac{\partial \rho}{\partial T} + \left( \frac{\partial n}{\partial T} \right)_\rho \right] \delta T + \left[ \left( \frac{\partial n}{\partial \rho} \right)_C \frac{\partial \rho}{\partial C} + \left( \frac{\partial n}{\partial C} \right)_\rho \right] \delta C \quad (3a)$$

$$\delta k = \left[ \left( \frac{\partial k}{\partial \rho} \right)_T \frac{\partial \rho}{\partial T} + \left( \frac{\partial k}{\partial T} \right)_\rho \right] \delta T + \left[ \left( \frac{\partial k}{\partial \rho} \right)_C \frac{\partial \rho}{\partial C} + \left( \frac{\partial k}{\partial C} \right)_\rho \right] \delta C \quad (3b)$$

where  $\rho$  is density of the solution. Since both Eqs. (3a) and (3b) are linear, the relationship between  $I_{TG}(t)$  and  $\delta T$ ,  $\delta C$  should be also linear. By solving the diffusion rate equations, the space and time behavior of both  $\delta T(x, t)$  and  $\delta C(x, t)$  can be obtained as exponential functions. Therefore, the following relationship is obtained:

$$I_{TG}(t) = \alpha T_0 \exp(-D_T q^2 t) + \beta C_0 \exp(-D_C q^2 t) \quad (4)$$

where  $D_T$  and  $D_C$  are the thermal diffusion coefficient of solution and concentration diffusion coefficient of solute molecule, respectively;  $\alpha$  and  $\beta$  are constants.  $T_0$  and  $C_0$  are the initial values of the raised temperature and excited molecular concentration just after excitation ( $t=0$ ).  $q$  is the grating constant described by the grating period ( $\Lambda$ ) as  $q=2\pi/\Lambda$ . Thus, time-profiles of the TG signals are predictable from this equation. Usually thermal diffusion processes are much faster than concentration diffusion processes ( $D_T \gg D_C$ ) in

solutions. Therefore, the fast and slow decay components in Fig. 3 should be attributed to the thermal and concentration grating components, respectively. This explains why observed thermal grating signal has a positive sign whereas the concentration grating signal has a negative sign.

In this case, the thermal grating only contributes to  $\delta n$ , and  $(\partial n/\partial T)_p$  term in Eq. (3a) is negligible. Also,  $(\partial n/\partial \rho)_T(\partial \rho/\partial T) < 0$  should be satisfied because solution densities generally decrease with increasing temperature. Thus,  $\delta n(t)$  in Eq. (2) should have a negative sign when the observed thermal signal has a positive sign. This suggests that  $\cos(\Delta\phi) < 0$  in Eq. (2). On the other hand, the concentration grating in this solution mainly contributes to  $\delta k$  because MF has large absorbance at the probe wavelength (633nm). In contrast, the contribution of SF is negligible because the absorption band of SF is located at the UV wavelength region. This fact has been reported using homodyne<sup>24-25</sup> and heterodyne<sup>18</sup> detected TG technique. Since molecular absorbance has a positive sign,  $\delta C(t)$  in Eq. (2) should have a positive sign while observed thermal signal has a negative sign. This suggests that  $\sin(\Delta\phi) < 0$ . Therefore, it is concluded that  $180^\circ < \Delta\phi < 270^\circ$ . The metal grating provides a permanent amplitude grating, which has  $180^\circ$  phase difference to the transient amplitude grating. The low absorbance regions of the metal grating (window) correspond to the high absorbance regions of the transient grating, because MF molecules were generated at these regions by the photochemical excitation. The other phase shift should be due to the optical pass length difference provided by the 100 nm thick metal grating film. This phase shift ranges between  $0^\circ$  to  $90^\circ$ , which seems reasonable because metal film thickness (100 nm) is smaller than 1/4 of the probe wavelength (633 nm). By changing the metal film thickness,  $\delta n(t)$  or  $\delta k(t)$  can be clearly

separated with  $\Delta\phi = 0^\circ, 180^\circ$  or  $90^\circ, 270^\circ$ , respectively. The controlling of  $\Delta\phi$  is also available by the previous techniques,<sup>13-21</sup> however,  $\Delta\phi$  was very unstable. By using our technique,  $\Delta\phi$  is almost permanently stable and still easy to control.

Since the decay time-scale of  $\delta T$  and  $\delta C$  are so different, each decay profile can be fitted by a single exponential function. Figure 4 depicts the semi-log plot of the corresponding time-profiles of  $\delta T(t)$  and  $\delta C(t)$ . Each profile shows a good exponential decay and the straight lines are fitted lines. By each signal decay rate,  $D_T$  and  $D_C$  are obtained as  $D_T = 7.1 \pm 0.5 \times 10^{-8} \text{ m}^2\text{s}^{-1}$  and  $D_C = 3.0 \pm 0.2 \times 10^{-10} \text{ m}^2\text{s}^{-1}$ .  $D_T$  can be calculated by the thermal conductivity ( $\kappa$ ), heat capacity ( $C_p$ ), and  $\rho$  as  $D_T = \kappa/\rho C_p$ . The calculated value of  $D_T$  of 2-propanol is  $D_T = 6.8 \times 10^8 \text{ m}^2\text{s}^{-1}$ . The experimentally obtained  $D_T$  value is very close to the calculated value.  $D_C$  of MF in 2-propanol was previously obtained by the homodyne TG technique as  $D_C = 2.7 \times 10^{-10} \text{ m}^2\text{s}^{-1}$ .<sup>25</sup> This value also agrees with  $D_C$  obtained by MPT-TG here. Theoretically, concentration diffusion coefficients are given by the following Stokes-Einstein equation with solute molecular radius ( $r$ ), solvent viscosity ( $\eta$ ), Boltzman constant ( $k_B$ ), and  $T$ :

$$D_{SE} = \frac{k_B T}{a \eta r} \quad (5)$$

where  $a$  is the constant that denotes a boundary condition between solute and solvent. This depends on the molecular size/shape, solvent structure, and solute-solvent interaction, etc., and usually ranges between  $4\pi$  (slip boundary) to  $6\pi$  (stick boundary).

The calculated  $D_{SE}$  values with slip and stick condition are  $3.8 \times 10^{-10} \text{ m}^2 \text{ s}^{-1}$  and  $2.5 \times 10^{-10} \text{ m}^2 \text{ s}^{-1}$ ,

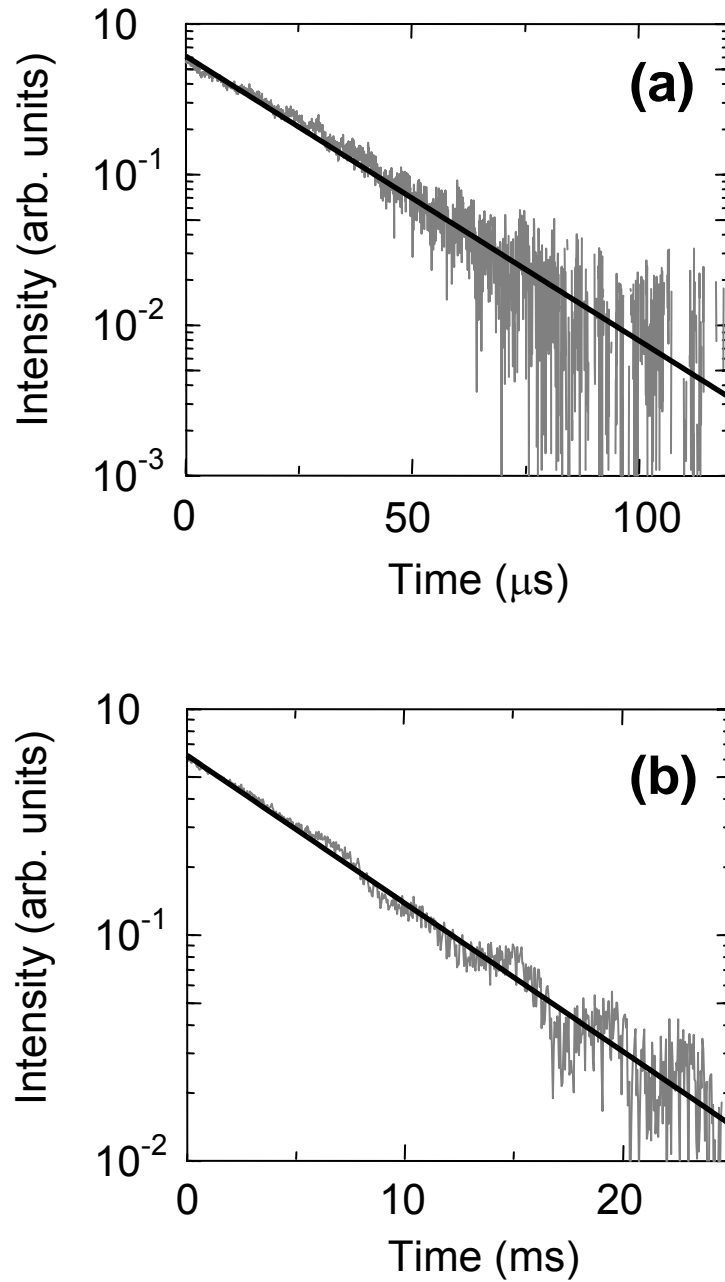


Fig. 4; Semi-log plots of the TG signals in microsecond timescale (a) and in millisecond timescale (b). The straight lines are best fits.

respectively. The obtained  $D_C$  value by MPT-TG is rather close to  $D_{SE}$  with the stick condition. This fact has been already reported elsewhere.<sup>18, 24</sup> The MF of spiropyran has a large dipole moment due to the intramolecular charge separated feature as shown in Fig. 2. This property causes a strong intermolecular interaction with polar solution molecules such as 2-propanol.<sup>25</sup> Such a strong interaction would bring a stick boundary condition between solute and solvent. Accordingly, we concluded that both the obtained  $D_T$  and  $D_C$  values are reasonable.

## Conclusion

We used the MPT-TG technique for spiropyran in 2-propanol solution to observe the chemical reaction and molecular dynamics. We measured  $D_T$  and  $D_C$  values by the time-profile of the TG signal. Both observed values are in good agreement with the calculated value or/and a previous reported value. The MPT-TG technique has the same advantages as the usual OHD-TG techniques such as high sensitivity, good analyzability, and a linear relationship of signal intensity versus  $\chi^{(3)}$ . Moreover, this technique's merits also include a very simple setting, easy alignment, and excellent phase stability. Also  $\Delta\phi$  should be controlled accurately by changing the metal grating thickness. The MPT-TG technique is expected to find broad applications in physics, chemistry, material, and biological study.

**References**

- <sup>1</sup>H. J. Eichler, P. Gunter, and D. W. Pohl, *Laser-Induced Dynamic Grating*, Springer, Berlin, 1986.
- <sup>2</sup>K. A. Nelson and M. D. Fayer, *J. Phys. Chem*, 72, 5202, 1980.
- <sup>3</sup>L. Genberg, Q. Bao, S. Gracewaski, and R. J. D. Miller, *Chem. Phys.* 131, 81, 1989.
- <sup>4</sup>M. Terazima, K. Okamoto, and N. Hirota, *J. Phys. Chem*, 97, 5188, 1993.
- <sup>5</sup>L. Dhar, J. A. Rogers, and K. A. Nelson, *Chem. Rev.* 94, 157, 1994.
- <sup>6</sup>J. A. Rogers and K. A. Nelson, *J. Appl. Phys.* 75, 1534, 1994.
- <sup>7</sup>K. Okamoto, M. Terazima, N. Hirota, *J. Chem. Phys.* 103, 10445, 1995.
- <sup>8</sup>K. Okamoto, N. Hirota, M. Terazima, *J. Phys. Chem. A.* 101, 5269, 1997.
- <sup>9</sup>M. Terazima, *Res. Chem. Intermed.* 23, 853, 1997.
- <sup>10</sup>K. Okamoto, N. Hirota, M. Terazima, T. Tominaga, *J. Phys. Chem. A.* 105, 6586, 2001.
- <sup>11</sup>P. Vöhringer, N.F. Scherer, *J. Phys. Chem.* 99, 2684, 1995.
- <sup>12</sup>W. Kohler, P. Rossmanith, *J. Phys. Chem.* 99, 5838, 1995.
- <sup>13</sup>J.A. Rogers, M. Fuchs, M.J. Banet, J.B. Hanselman, R. Logan, K.A. Nelson, *Appl. Phys. Lett.* 71, 225, 1997.
- <sup>14</sup>A.A. Maznev, K.A. Nelson, J.A. Rogers, *Opt. Lett.* 23, 1319, 1998.
- <sup>15</sup>G.D. Goodno, G. Dadusc, R.J.D. Miller, *J. Opt. Soc. Am. B.* 15, 1791, 1998.
- <sup>16</sup>Q.-H. Xu, Y.-Z. Ma, G. R. Fleming, *Chem. Phys. Lett.* 338, 254, 2001.
- <sup>17</sup>M. Terazima, *Chem. Phys. Lett.* 304, 343, 1999.
- <sup>18</sup>M. Terazima, *J. Phys. Chem. A*, 103, 7401, 1999.
- <sup>19</sup>K. Katayama, M. Yamaguchi, and T. Sawada, *Appl. Phys. Lett.* 82, 2775, 2003.
- <sup>20</sup>M. Yamaguchi, K. Katayama, and T. Sawada, *Chem. Phys. Lett.* 377, 589, 2003.
- <sup>21</sup>K. Katayama, M. Yamaguchi, and T. Sawada, *J. Appl. Phys.* 94, 4904, 2003.

<sup>22</sup>K. Okamoto, Z. Zhang, A. Scherer, D. T. Wei, *Appl. Phys. Lett.* 85, 4842, 2004.

<sup>23</sup>K. Okamoto, Z. Zhang, D. T. Wei, A. Scherer, *Thin Solid Films*, 469–470, 420, 2004.

<sup>24</sup>T. Okazaki, N. Hirota, and M. Terazima, *J. Photochem Photobiol.* 99, 155, 1996.

<sup>25</sup>K. Okamoto, N. Hirota, M. Terazima, *to be published*

## Chapter 7–Molecular filter-nanosieve

### Abstract

Demonstrated in this paper is a molecular sieve. The focus of this work is making a “smart” filter. This filter has electrochemical and electromechanical properties that would allow both sorting and filtering of solutions. Prior sifters and sieving structures have been at the mercy of a static material structure, whereas the convention proposed here allows dynamic control of filtering size during an assay.

The filter mechanism simply relies on a sandwiched layer of oxide, grown in an RF sputtering system. This allows for almost Angstrom-level control of the thickness. An oxide layer is sandwiched between two layers of silicon with e-beam written holes 100 nm in diameter, one offset from the other. Dry etching is used to carve these holes in the silicon layers, and wet oxide etching defines a void in the sandwiched layer. The distance that the two silicon layers are separated dictates the smallest filtering size.

Analysis is available through several methods. Mechanically, a fluid can be passed through the holes carrying along with it the particles or molecules that are small enough to make it through the oxide layer. Electrochemically, a charged particle can be placed on one side of a container and separated by the filter. The charged particle would then have the tendency to go to the other side, given a concentration gradient, and thereby pass through the filter [1].

## Introduction

The analysis of small volumes of solutions is extremely important for many biological applications. The goal of this work is to define small cavities that can be used to filter sub-100 nm particles and even molecules. Here we present the design and fabrication details of such filters, as well as preliminary experimental results.

## Theory

Sputtering and etching are common processes that are used in microelectronics microfabrication, but can be applied to the nanofabrication of fluidic devices. Using these processes for new areas offers the opportunity for combining the excellent

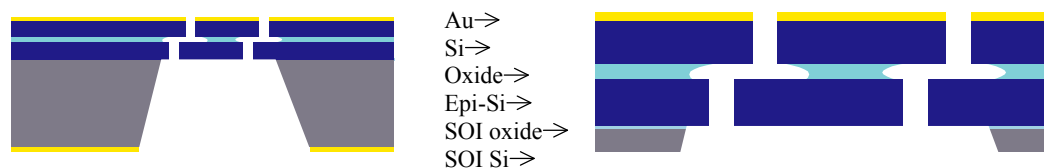


Figure 1. Illustration of nanosieve, left, and close-up on the right, with a thin gold film evaporated on both sides of the substrate. (Layers not drawn to scale.)

dimensional control from the microelectronics industry with the massive integration of miniaturized devices on a monolithic substrate. That is why we seek to fabricate our nanosieve lithographically. However, even with the excellent capabilities of high-resolution lithography, it is very difficult to define hole sizes below 10 nm with adequate uniformity for high-quality filtration. Therefore, it is desirable to define filters in which the geometric size of the constriction is controlled by growth rather than by lithography. Here we demonstrate such a geometry, in which we use the vertical control over layer thickness to determine the filter size, and provide access to this constriction by

lithographically defined holes. To define the filter, we use two steps of electron beam lithography and dry etching with multiple alignments to obtain offset holes within two thin silicon membranes, which are connected through a sacrificial silicon dioxide layer that ultimately controls the filter size. Since the layer thickness of a sacrificial layer can be controlled to within less than 1 nm during the construction of the filter, it is possible to accurately set the filter geometry and control the size of particles or molecules that can pass through the filter.

## **Experimental**

The fabrication sequence is summarized in Figure 1, where we show the steps that are needed for defining our lithographic filter. First, we use electron beam lithography to define an array of holes on a silicon on insulator (SOI) sample. The thickness of the silicon layer is approximately 200 nm, whereas the SOI oxide thickness is approximately 400 nm. We use polymethylmethacrylate (PMMA) as an electron beam resist, as well as an etch mask. Using a chemically assisted ion beam etching system (CAIBE) with  $\text{XeF}_2$  reactive gas, the pattern written using e-beam lithography, illustrated in Figure 2, is etched through the first silicon layer. The beam voltage and other parameters are set appropriately in order to maintain an acceptable etch ratio between the etch mask layer and the silicon. Following this procedure, the etched holes are filled with gold, and the PMMA is removed in acetone. Then, a precisely controlled silicon dioxide sacrificial layer is sputtered onto the sample, followed by a thicker polycrystalline silicon layer. Another lithography procedure is then used to define a similar array of holes, with a small offset, on top of the original hole structure. Finally, hydrofluoric acid and gold etch are

used to define the connection between the lithographically defined holes through the silicon dioxide sacrificial layer.

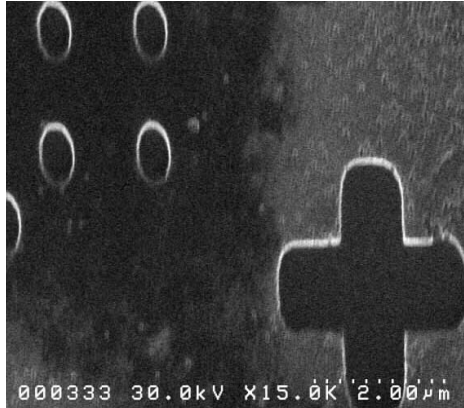


Figure 2. SEM view of e-beam-written, etched holes and alignment mark used for offsetting the top layer.

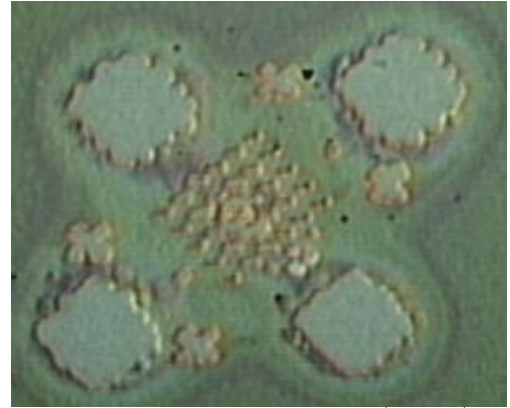


Figure 3. Suspended epi-Si membrane with e-beam-written holes in the center.

We observe the hole size increase over the lithographic pattern by a few tens of nanometers in diameter after the etching process. This increase in pattern size can be adjusted for during the design of the filter by spacing the holes appropriately farther apart. Thus, the sputtered oxide thickness and wet etching, using a buffered HF solution, creates the geometric structure of the filter. Objects exceeding the size of the void are not allowed to pass through, and the accuracy over the filter size is determined only by the control over the deposited thickness of the oxide.

In our device, gold is used to fill in the holes. Often, chromium or titanium layers are used to allow for adhesion to the substrate. However, adequate sidewall adhesion can be achieved in our structures by evaporating at a low rate  $<10$  Angstroms/sec during the first several tens of nanometers. In addition, we have observed that timing is essential in ensuring that the gold lift-off process is successful.

## **Results and discussion**

Fabrication of a lithographically defined filter is achieved through careful processing. More fabrication issues are encountered during the analysis. One convention looks to allow molecules or colloidal beads to pass through by way of a backside etch. Another convention, illustrated in Figure 3, would better suit the needs for mass scale production by allowing access to the bottom side of the filter from the top of the substrate. Undercutting the buried oxide layer in the SOI substrate allows access to the backside of the e-beam-written holes.

Both conventions will require sub-micro-scaled fabrication on top of the surface, whereas the primer would necessitate maneuvering of the sample in order to access the backside. These techniques are currently being explored.

## **Conclusions**

Fabrication limits are approached when seeking to demonstrate filtration through a surface machined silicon on insulator fluidic channel. The high uniformity and large areas needed for filter action require the use of new geometries to ensure accurate definition of filter elements that can be used for biological assays. Use of fluorescent beads and fluorescently labeled molecules will be used to determine the quality of our filter. Meanwhile, the fabrication approach towards producing a filter in which the control over geometry is assured by deposition has been demonstrated. These devices will be able to be integrated into microfluidic analysis systems.

**Reference**

- [1] Jiali Li, Derek Stein, Ciaran McMullan, Daniel Branton, Michael J. Aziz, Jene A. Golovchenko. “Ion-beam sculpting at nanometer length scales” **Nature**. 412. 166–129, 2001.

## **Chapter 8–Photo-oxidation competes with surface plasmon coupling**

### **Abstract**

Organic light emitters have lagged behind inorganic light emitters in terms of overall efficiency. In lieu of device stability issues in an oxygen atmosphere, we show how this efficiency can be increased by use of surface plasmon coupling. Surface plasmons outperform nitrogen in photo-oxidation studies. We have demonstrated a way to extend the lifetime of organic light emitters by reducing the photodegradation effects from photo-oxidation using surface plasmon coupling.

## **Introduction**

During PL measurements of polyfluorene based organic light emitters we observed photodegradation effects. Initially, it was thought that the main contributor in the photodegradation was photo-oxidation. Photo-oxidation happens initially at the surface and that is where the surface plasmons supported by the metal film compete. Several studies looking at failure of the polymeric light emitting devices,<sup>1</sup> oxidative degradation of the active polymer layer,<sup>2</sup> and studies of how photo-oxidation, resulting in delamination of the polymer from the metal surface,<sup>3</sup> affects the optical properties of the conjugated polymer have been pursued. Other studies have compared PL measurements in nitrogen atmosphere to those in an oxygen atmosphere and shown that the intensity is higher in the nitrogen atmosphere.<sup>4</sup> Extensive studies using photoabsorption spectroscopy look at exactly where the photo-oxidation occurs.<sup>5</sup> Gold presented a summary focusing on the short lifetimes of light emitting polymers.<sup>6</sup> In particular, the lifetime of the light emitting polymers based on polyfluorenes has been shown to be affected by photo-oxidation.<sup>7</sup>

## **Experiment**

The samples were prepared by evaporating 50 nm of silver on half of a quartz slide. A 2% by volume conjugated polymer, polyfluorene, 100-200 nm was spun on the half coated quartz sample. The pump light excited the sample from oblique incidence. The detector was positioned in front of the sample after focusing lenses. For comparison, a tube was placed near the sample to flood with nitrogen. The flow of nitrogen across the sample during the PL measurement is referred to here as the nitrogen effect. When the conjugated polymer is placed on metal, the PL measurement is referred to as the surface

plasmon effect. Measurements were taken to compare the nitrogen and surface plasmon effect.

The initial measurement, shown in Figure 1, is the time profile of the photoluminescence (PL) intensity of the conjugated polymer on metal and on bare quartz. We observed a slower decay of the PL intensity for the conjugated polymer on metal.

In Figure 2, we show the data obtained from the nitrogen effect alone of PL measurements with and without nitrogen flowing for the conjugated polymer on bare quartz.

The combined effects we can observe in Figure 3 where the PL intensity decay for the conjugated polymer on bare quartz is compared with the conjugated polymer on metal, both with nitrogen flowing.

## Results and Discussion

We may use the following equation to offer a description of the mechanism:

$$\eta_{ox} = \frac{k_{ox}}{k_{rad} + k_{non} + k_{ox} + k_{sp}}$$

where  $\eta_{ox}$  is the internal quantum efficiency for oxidative processes,  $k_{non}$  is the nonradiative recombination rate,  $k_{rad}$  radiative recombination rate,  $k_{ox}$  oxidation rate, and  $k_{sp}$  surface plasmon recombination. Initially  $k_{sp}$  dominates the equation as electromagnetic fields are strongest close to the metal film and the oxidative process is reduced. As you extend into the conjugated polymer material, farther away from the metal film,  $k_{ox}$  becomes the dominate process and oxidation happens more readily.

A slower PL intensity decay is observed with surface plasmon coupling alone. Also, a slower decay is observed with both surface plasmon coupling and with flowing nitrogen. After a long time, the surface plasmon coupling keeps the PL intensity strong.

### **Conclusions**

We expect encapsulated devices with a thin metal layer to allow for the surface plasmon effect to increase the overall stability of organic light emitting devices and extend their lifetime. We have demonstrated a way to extend the lifetime of organic light emitters by reducing the photodegradation effects from photo-oxidation using surface plasmon coupling.

Figure 1

Surface Plasmon Effect without nitrogen flowing.

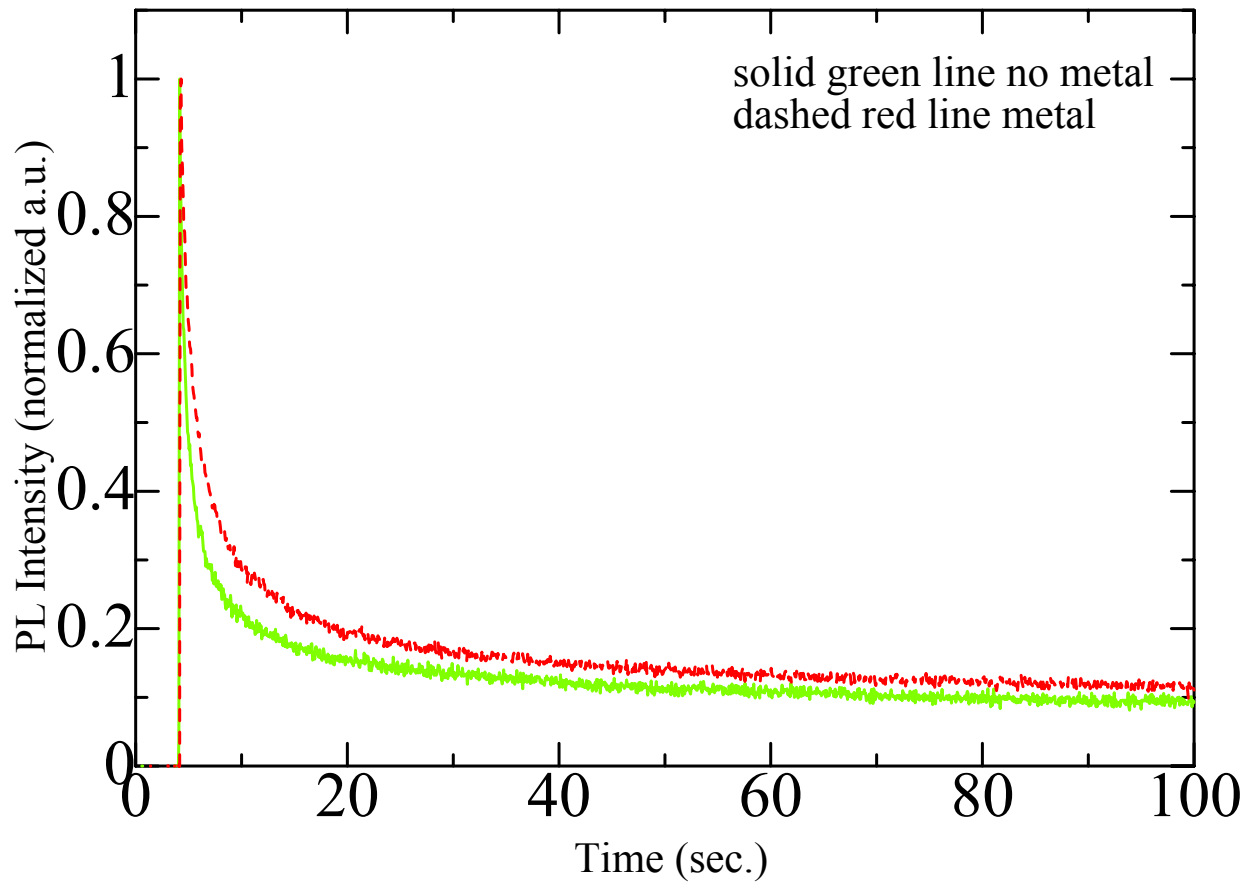


Figure 2

Nitrogen Effect illustrating the PL intensity decay of the conjugated polymer on bare quartz with nitrogen flowing.

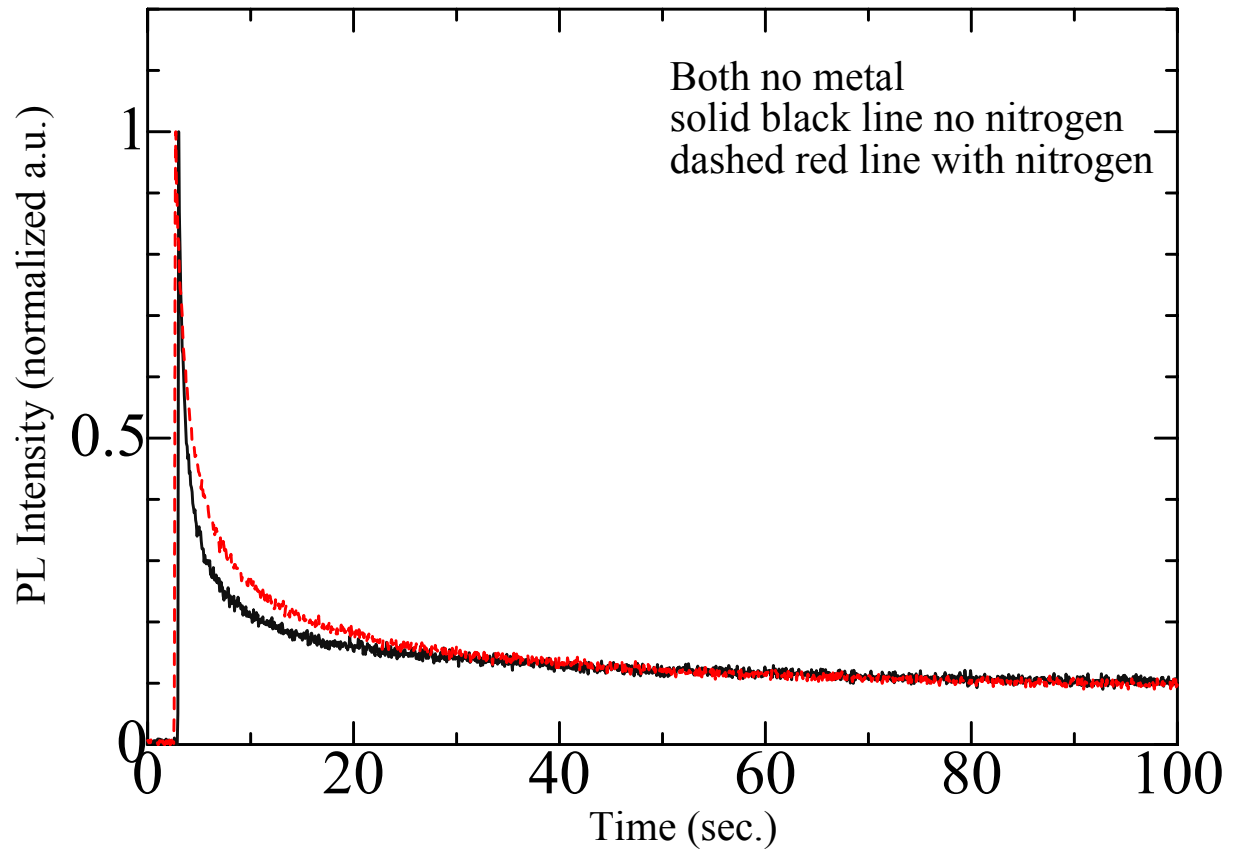
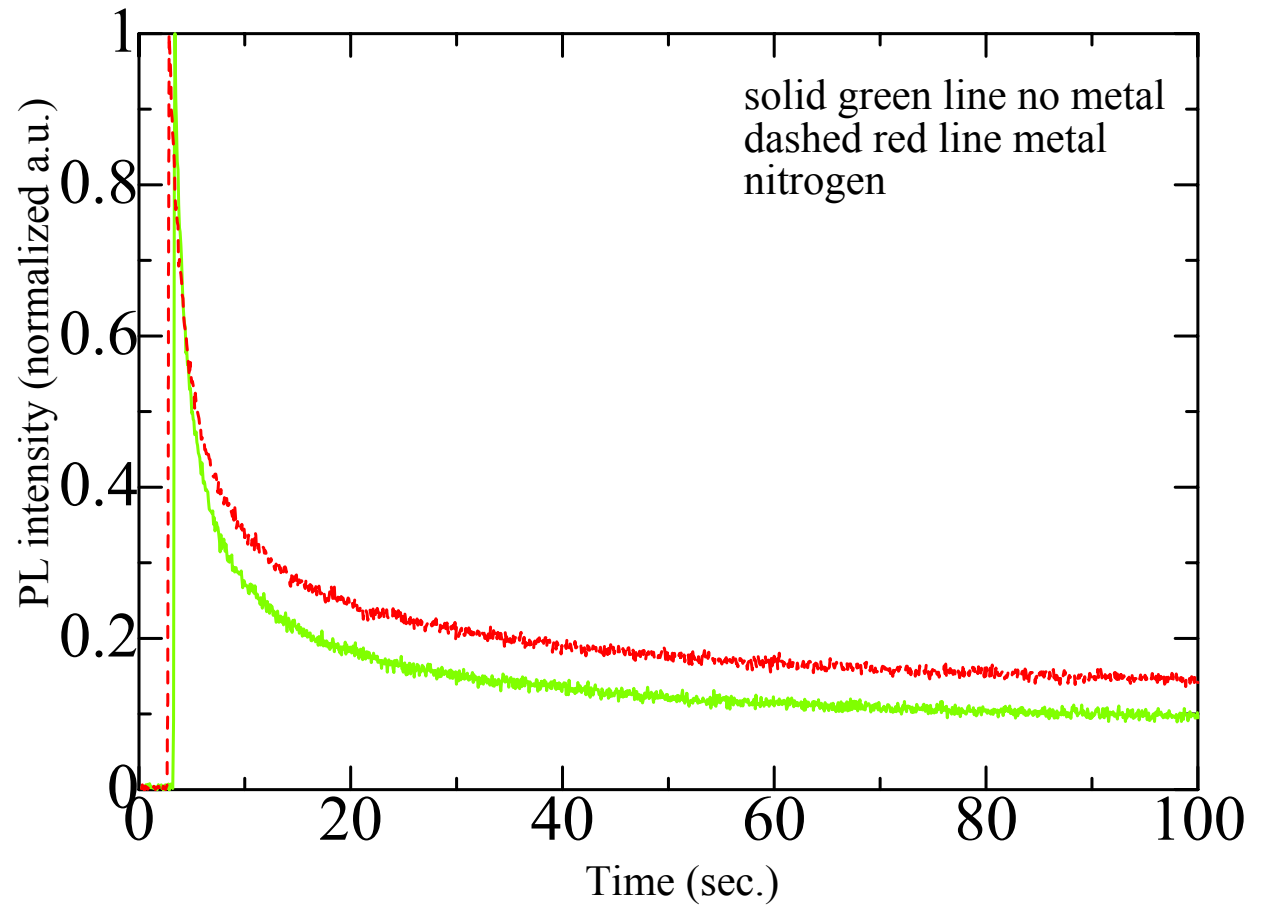


Figure 3

Surface Plasmon Effect and Nitrogen Effect.



**References**

- <sup>1</sup>B. H. Cumpston and K. F. Jensen, *Appl. Phys. Lett.* 69, 25, 1996.
- <sup>2</sup>B. H. Cumpston, I. D. Parker, and K. F. Jensen, *J. Appl. Phys.* 81, 8, 1997.
- <sup>3</sup>V. N. Savvat'ev, A. V. Yakimov, D. Davidov, R. M. Pogreb, R. Neumann, Y. Avny, *Appl. Phys. Lett.* 71, 23, 1997.
- <sup>4</sup>M. Yan, L. J. Rothberg, F. Papadimitrakopoulos, M. E. Galvin, and T. M. Miller, *Phys. Rev. Lett.* 73, 5, 1994.
- <sup>5</sup>D. G. J. Sutherland, J. A. Carlisle, P. Elliker, G. Fox, T. W. Hagler, I. Jimenez, H. W. Lee, K. Pakbaz, L. J. Terminello, S. C. Williams, F. J. Himpsel, D. K. Shuh, W. M. Tong, J. J. Jia, T. A. Callcott, and D. L. Ederer, *Appl. Phys. Lett.* 68, 15, 1996.
- <sup>6</sup>J. F. Gold, *Literature Survey at University of Cambridge*, 1997.
- <sup>7</sup>X. Gong, P. K. Iyer, D. Moses, G. C. Bazan, A. J. Heeger, S. S. Xiao, *Advanced Functional Materials* 13, 4, 2003.

## **Chapter 9–Geometry in sync with surface plasmon coupling**

### **Abstract**

Entrenched metal grating structures were fabricated. Peak photoluminescence intensities from a conjugated polymer on particular grating structures were measured. Investigations on how to synchronize metal geometry with surface plasmon coupling for enhanced device efficiency were performed.

## **Introduction**

The work focused on here is to study geometry's role in the manipulation of light using metals. In particular, grating structures are used to excite surface plasmons. The roughness of the metal film was the topic of discussion in Chapters 3 and 4. In this chapter, the influence of the metal films is the focus.<sup>1</sup> Sun et. al. have performed light transmission studies to uncover the role of surface plasmons in the optical interaction in metallic gratings.<sup>2</sup> Theoretical work on modeling surface plasmons using structure surfaces and experimental verification of the designer surface plasmons have been explored.<sup>3-6</sup> One work reports an efficiency enhancement by patterning the aluminum cathode of an organic light emitting diode.<sup>7</sup> Mediated photoluminescence<sup>8</sup> as well as enhanced electroluminescence<sup>9</sup> has been observed for organic light emitters which have a corrugated structure on it allowing the coupling of surface plasmon modes and light to scatter from the rough metal layer. Strong emission and transmission from organic light emitters have been report for the cross coupling of surface plasmons between metal layers.<sup>10-11</sup>

## **Experiment**

There were two different configurations for the fabricated devices. One device has etched gratings in quartz filled in with metal and the other one consists of metal gratings on top of a quartz substrate. The metal used for these measurements was silver. The first type of device fabricated is described in Figure 1. During the electron beam writing process, gratings designed to have 50 nm, 75 nm, 100 nm, 125 nm, 150 nm, 175 nm, 200 nm, 300 nm, 400 nm, 500 nm, 600 nm, 700 nm, 800 nm, 900 nm spacings and twice that

number in pitch were exposed in the electron beam sensitive resist. After developing the electron beam written pattern, I used the ion mill process, where Argon plasma was used to transfer the electron beam written pattern into the metal layer. Next a series of etch steps to create trenches in the quartz substrate was performed first to etch the sacrificial spacer layer of polymethylmethacrylate (PMMA) and second to etch the quartz. To help facilitate the lift-off process, for the entrenched metal structures, the metal was evaporated at a slight angle, and then lift-off was performed in acetone.

Steps for fabricating the metal gratings on quartz were easier, as metal was first evaporated on quartz before applying the electron beam resist. After the electron beam writing and developing steps, one ion milling step transferred the pattern into the metal. Then acetone was used to remove the PMMA remnants of the sacrificial layers. A polyfluorene based conjugate polymer, pflcnp1, was spun on both samples and photoluminescence measurements performed.

Figure 1

Cartoon illustration of the fabrication process for the entrenched metal grating structures.

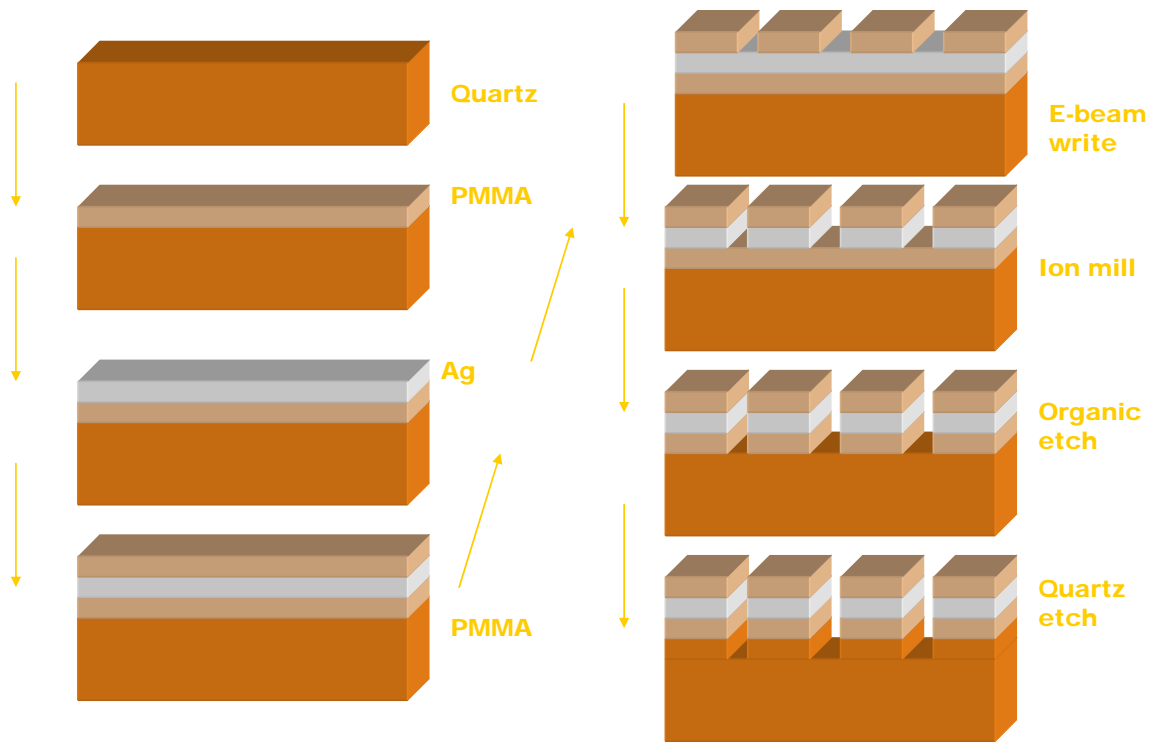


Figure 2

Entrenched grating structures before (above) and after liftoff (below).

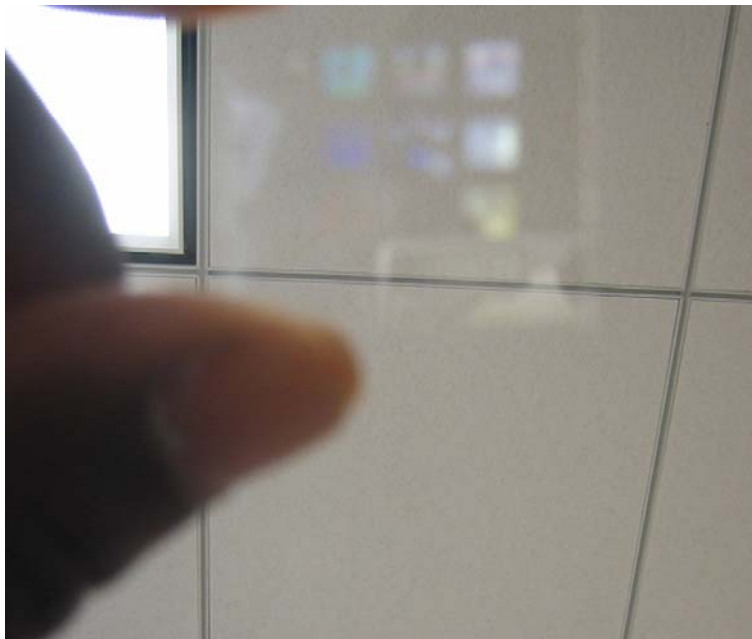


Figure 2 shows the entrenched metal quartz sample before and after liftoff. The sample illustrated has grating spaces of 200 nm to 900 nm, in the clockwise direction, starting from the bottom. The structures in the center of the sample were for calibration. The grating structures are still visible in the lower figure after the metal sacrificial layer was removed. The field size chosen, 3 mm by 3 mm, made it possible to measure the structures one at a time without the need of micro-photoluminescence.

I employed the use of a 405 nm InGaN diode laser to pump the light emitting polymer on grating samples. A Cooled CCD was used to measure the signal after first filtering it with an OD 200 neutral density filter. Plotted in Figure 3 is the maximum PL intensity for the conjugated polymer on entrenched metal grating sample. By comparison, in Figure 4, the normalized data for the peak PL intensity for the conjugated polymer on surface mounted metal gratings is shown. The peak values were considerably higher before normalizing as more metal was present to make up the gratings and there was more interaction between the conjugated polymer and metal, as the metal was on top of the substrate.

Although the data from both samples did not match directly, for the larger grating widths, namely structures on the order of the wavelength of light, the emission intensity enhancements were greater.

## **Results and Discussion**

I have presented a photoluminescence study of conjugated polymers based on the geometry of the metal on which the polymer is placed. Structures on the order of the wavelength of light showed the most enhancements.

I believe that the grating structures can serve a dual purpose, to enhance or extract light emission and be used for electrical contact.

Figure 3

Peak PL intensities of the conjugated polymer on the entrenched metal gratings fabricated.

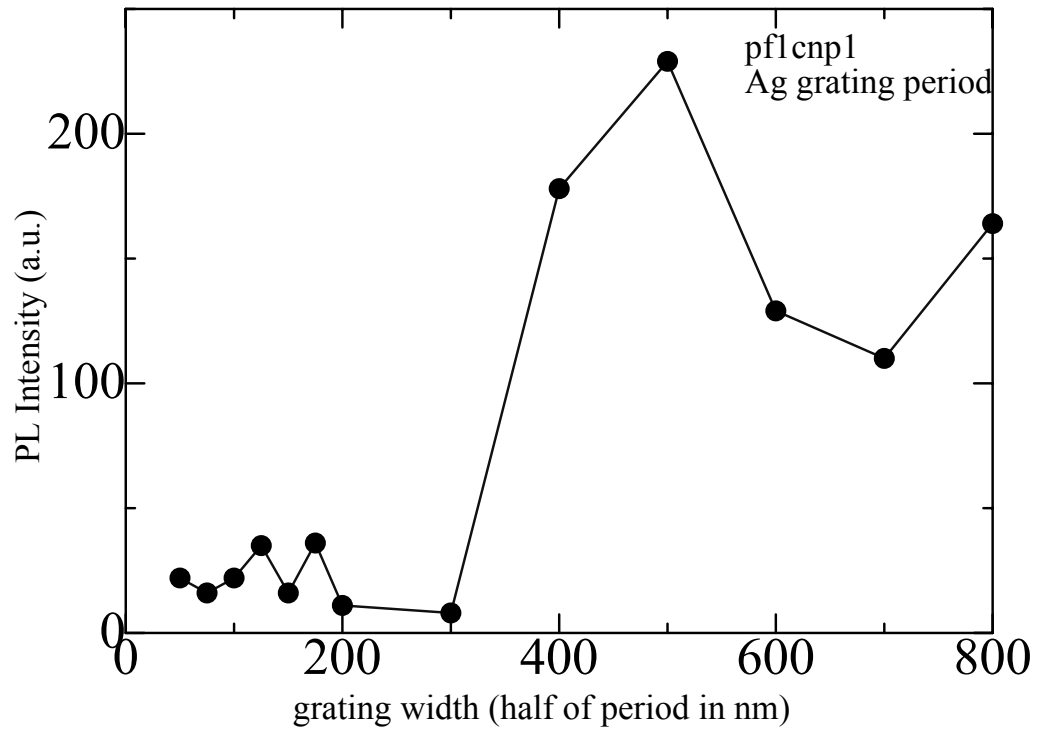
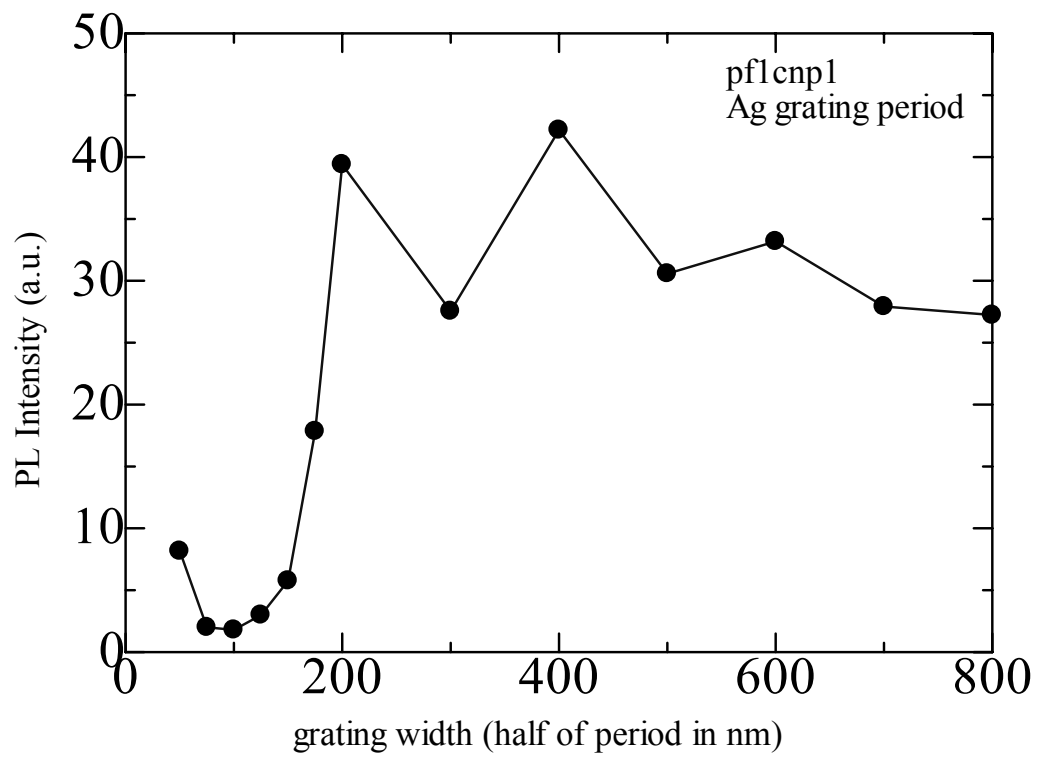


Figure 4

Peak PL intensities of the conjugated polymer on the surface mounted metal gratings fabricated (normalized).



**References**

- <sup>1</sup>S. Gianordoli, R. Hainberger, A. Köck, N. Finger, E. Gornik, C. Hanke, and L. Korte, *Appl. Phys. Lett.* 77, 15, 2000.
- <sup>2</sup>Z. Sun, Y. S. Jung, H. K. Kim, *Appl. Phys. Lett.* 83, 15, 2003.
- <sup>3</sup>J. B. Pendry, L. Martin-Moreno, and F. J. Garcia-Vidal, *Science* 305, 2004.
- <sup>4</sup>A. Giannattasio, S. Wedge, and W. L. Barnes, *J. of Modern Optics* 53, 4, 2006.
- <sup>5</sup>A. P. Hibbins, B. R. Evans, and J. R. Sambles, *Science* 308, 2005.
- <sup>6</sup>A. Neogi, C-W. Lee, H. O. Everitt, T. Kuroda, A. Tackeuchi, and E. Yablonovitch, *Phys. Rev. B* 66, 153305, 2002.
- <sup>7</sup>C. Liu, V. Kamaev, and Z. V. Vardeny, *Appl. Phys. Lett.* 86, 143501, 2005.
- <sup>8</sup>S. Wedge, J. A. E. Wasey, W. L. Barnes, and I. Sage, *Appl. Phys. Lett.* 85, 2, 2004.
- <sup>9</sup>J. Feng, T. Okamoto, and S. Kawata, *Optics Lett.* 30, 17, 2005.
- <sup>10</sup>D. K. Gifford and D. G. Hall, *Appl. Phys. Lett.* 81, 23, 2002.
- <sup>11</sup>D. K. Gifford and D. G. Hall, *Appl Phys. Lett.* 80, 20, 2002.

## Conclusion

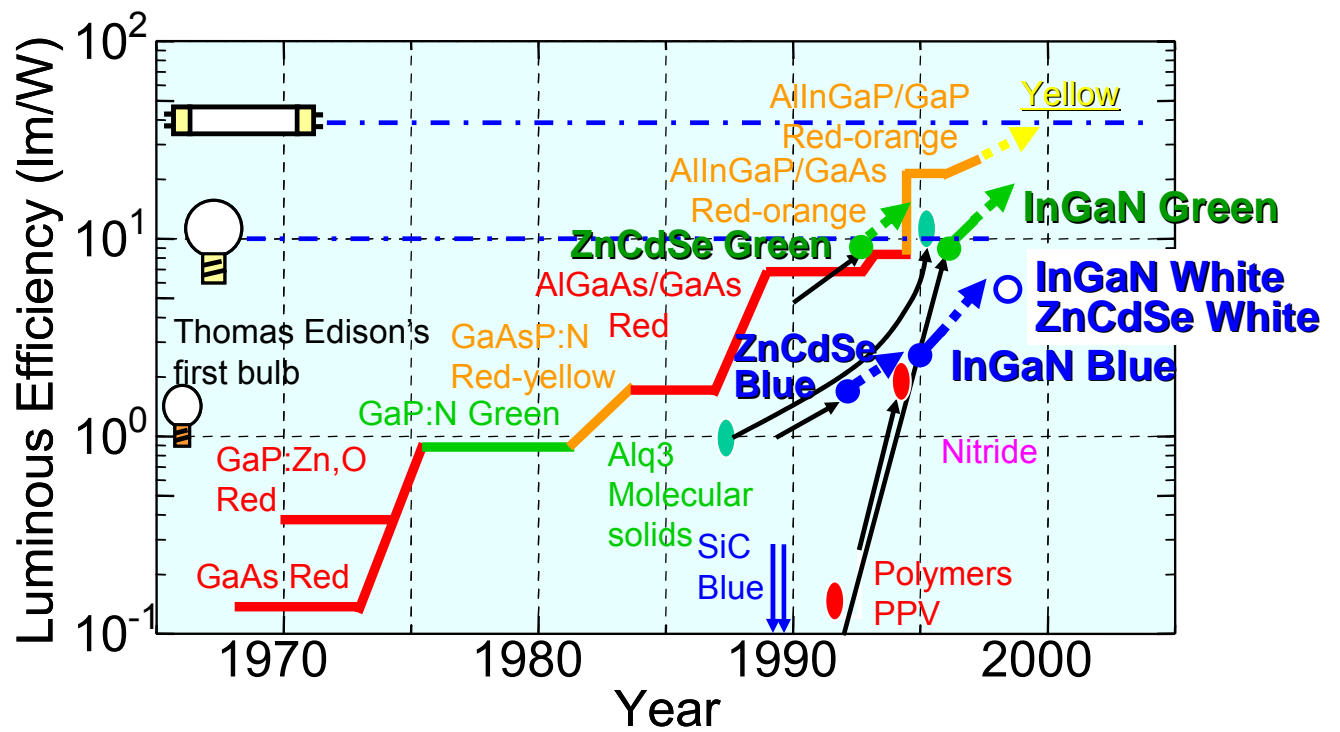
The MPT-TG technique is expected to find broad applications in physics, chemistry, material, and biological study. We have observed that the emission of dye-doped polymers can be enhanced by using surface plasmon coupling to thin metal layers. This study serves as a foundation for the geometric tuning of the surface plasmon resonance and enhancement of the emission of dye polymers using surface plasmons with patterned metal samples. If tuned properly, such lithographically structured layers should provide even higher enhancement values for the dye emission intensity. As the metallic surface can be used as an electrical contact, as a metallic grating for enhanced light extraction, and as a mirror for the definition of ultra-small optical cavities to further increase the spontaneous emission rates, we expect that many organic light-emitting diodes could benefit from careful design and choice of metallization. Ultimately, lithographic tuning of the peak emission wavelength and optimization of the polymer layer stack can also result in efficient white light source OLEDs. From studying the TRPL of these polyfluorenes in conjunction with the PL enhancement ratios we have found that those with longer carrier lifetimes offer large improvements in quantum efficiency if surface plasmons are used to enhance recombination of electron-hole pairs. Although only 3 or 4 times the emission enhancement is observed this is a significant increase in quantum efficiency from these state-of-the-art organic light emitters. We expect that, along with the development of robust and efficient polymers, the use of surface plasmons will ultimately lead to highly efficient polymer light emitters that can be used for solid state lighting applications.

## Appendices

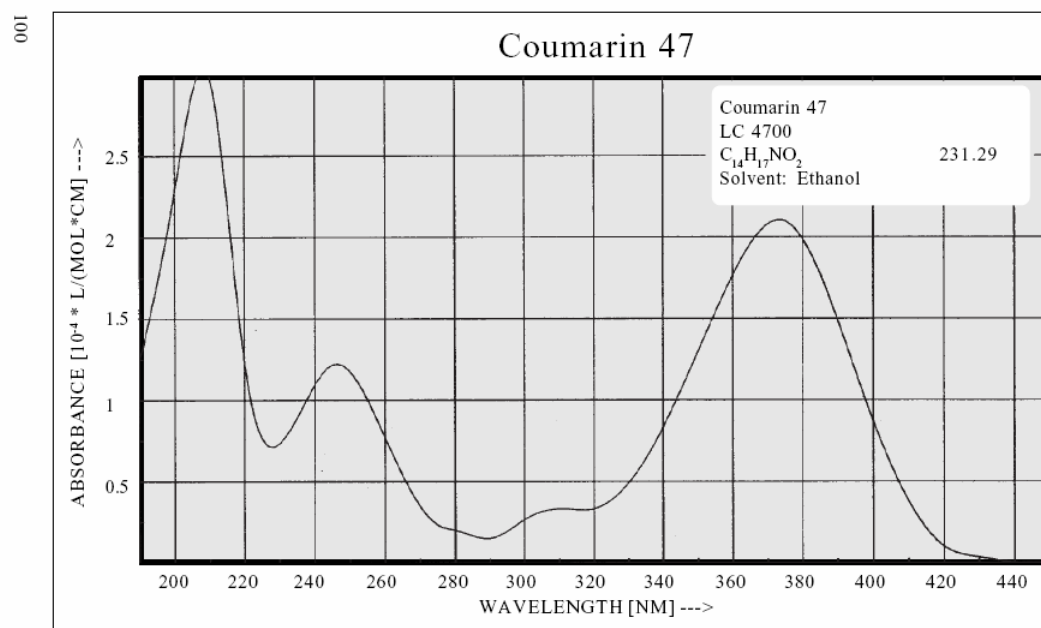
### Appendix A

#### LED Trend

Sheats, J., Antoniadis, H., Hueschen, M., Leonard, W., Miller, J., Moon, R., Roitman, D., and Stocking, A., *Science* 273, 884, 1996.



## Appendix B



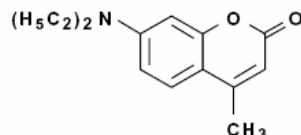
# Coumarin 47

---

## ■ Constitution:

7-Diethylamino-4-methylcoumarin  
Coumarin 460 · Coumarin 1

$C_{14}H_{17}NO_2$  · MW: 231.29



## ■ Characteristics:

Lambdachrome® number: ..... 4700  
 CAS registry number: ..... 99-44-1  
 Appearance: ..... slightly yellow, crystalline solid  
 Absorption maximum (in ethanol): ..... 373 nm  
 Molar absorptivity: .....  $2.10 \times 10^4 \text{ L mol}^{-1} \text{ cm}^{-1}$   
 Fluorescence maximum (in ethanol): ..... 450 nm  
 For research and development purposes only.

## ■ Lasing Performance:

Efficient laser dye for pulsed and CW operation; tunable around 450 nm.

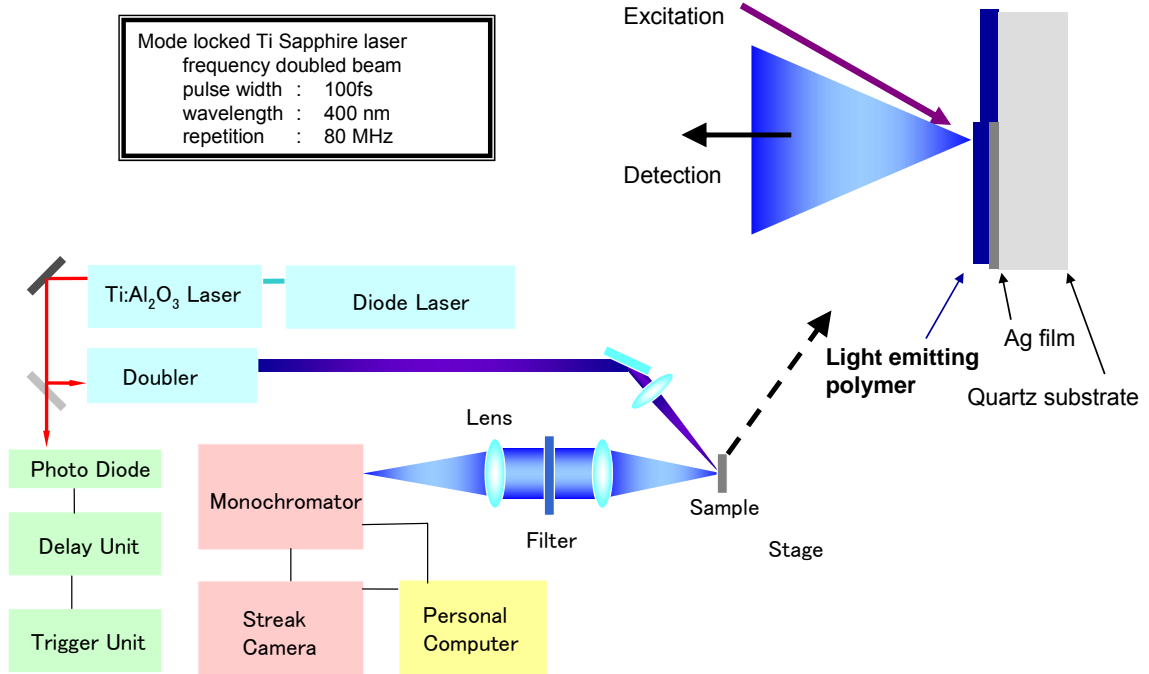
Source	Pump		Dye Laser Characteristics					
	Wavelength		Peak	Range	Effic.	Conc.	Solvent	Ref.
	[nm]		[nm]	[nm]	[%]	[g/l]		
XeCl-Excimer	308		456	440 - 484	18	1.60	Methanol	1, 2, 3
Nitrogen	337		453	436 - 486	rel.	0.66	Methanol	3, 4
Nd:YAG, 3rd	355		460	444 - 476	15	0.3	Methanol	1, 5
Flashlamp	-		460	435 - 490	-	0.02	Ethanol	6, 7
CW, Ar <sup>+</sup>	UV		470	450 - 500	-	1.76	MeOH/Eg.	8

## ■ References:

1. Lambda Physik, *Wall Chart* 96
2. H. Telle, W. Hüffer, D. Basting, *Opt. Commun.* **38**(5,6), 403 (1981)
3. F. Bos, *Appl. Optics* **20**(20), 3553 (1981)
4. Lambda Physik, *Data Sheet*
5. D. M. Guthals, J. W. Nibbler, *Opt. Commun.* **29**(3), 322 (1977)
6. J. B. Marling et al., *Appl. Optics* **13**(10), 2317 (1974)
7. J. B. Marling et al., *Appl. Phys. Letters* **17**(12), 527 (1970)
8. Coherent, *CW Dye Laser Fact Sheets*

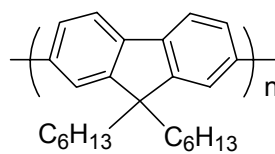
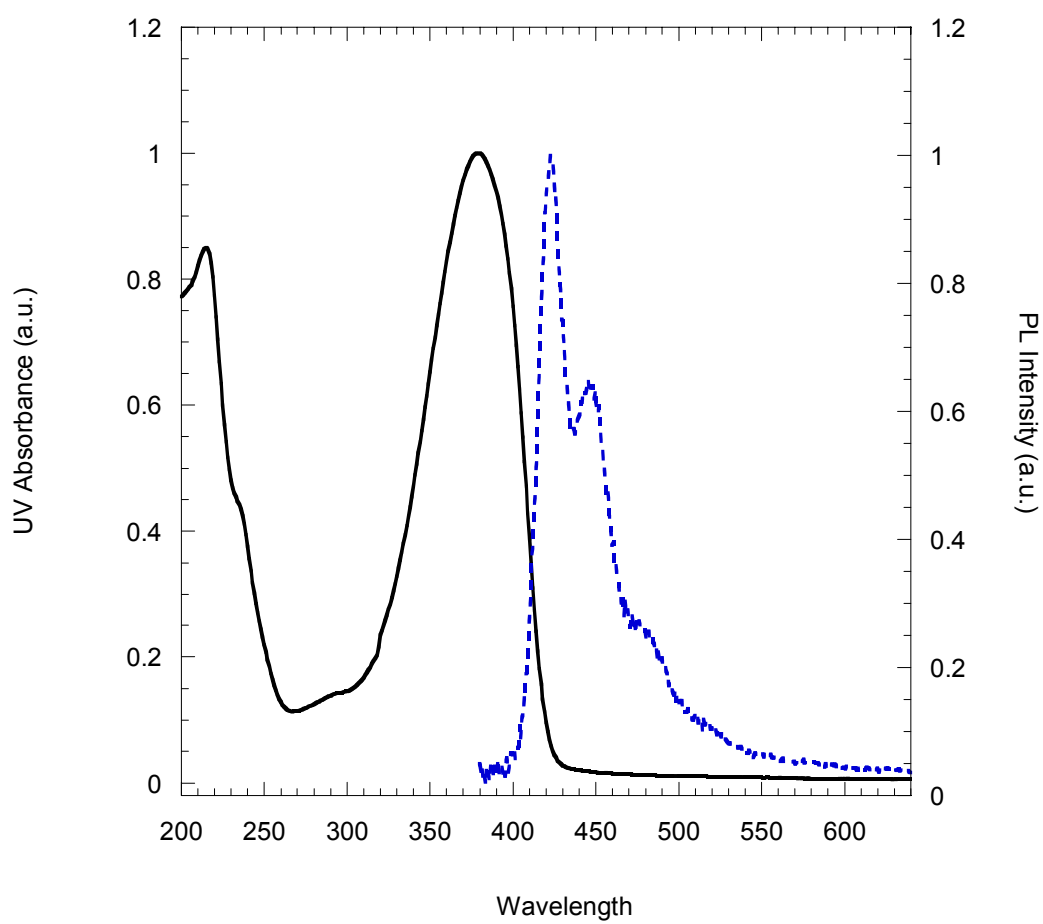
## Appendix C

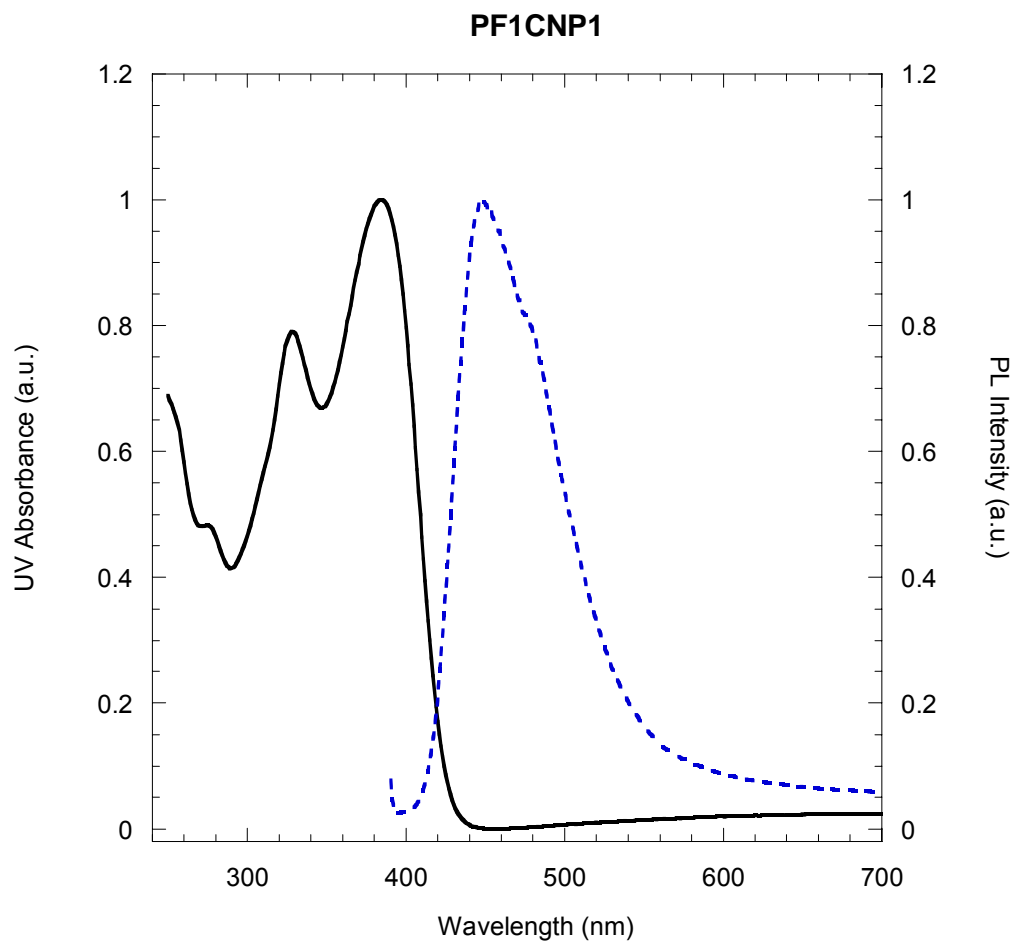
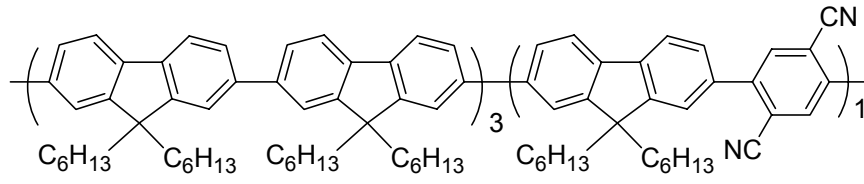
### Time-Resolved Photoluminescence Measurement w/ Hamamatsu Photonics C4334 Streak Camera

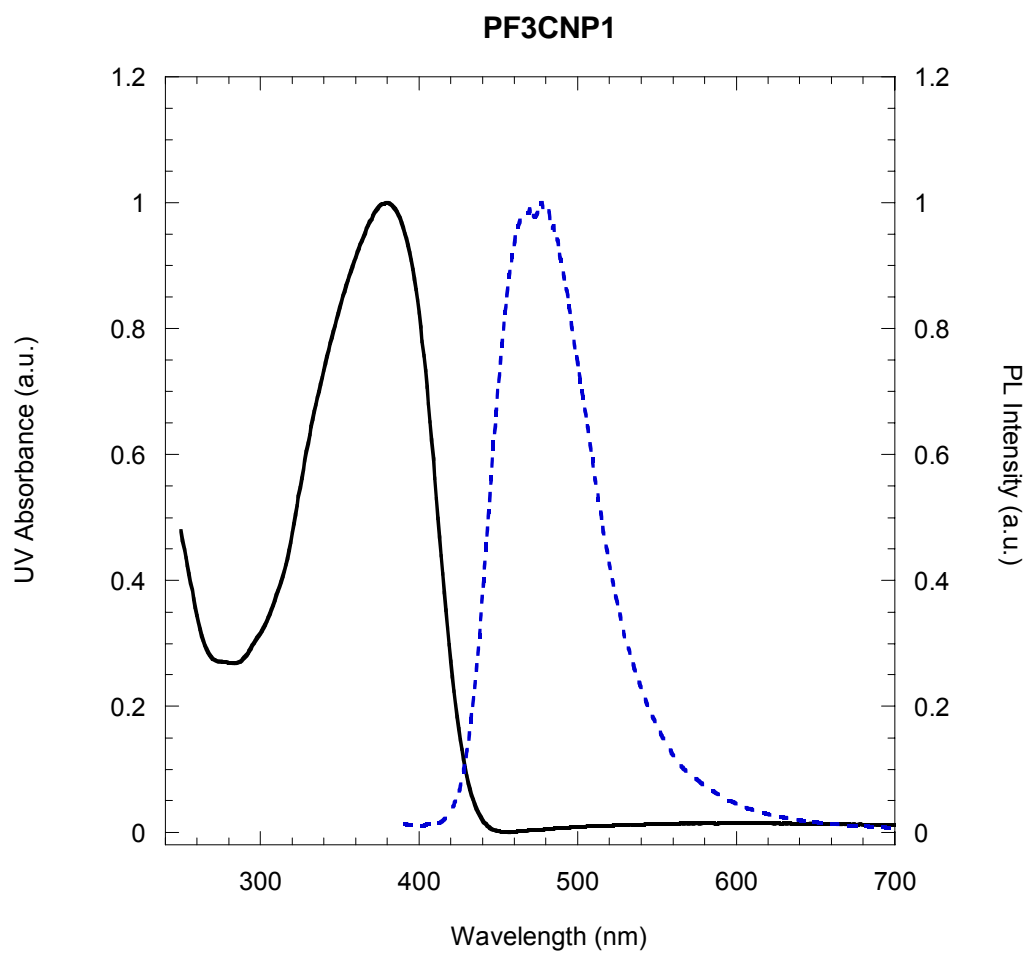
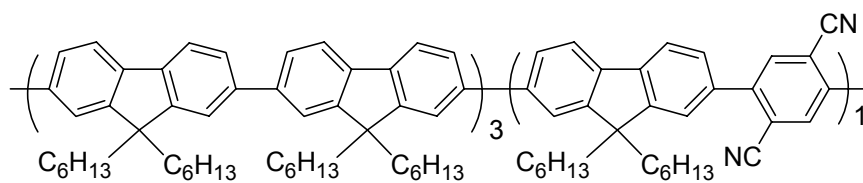


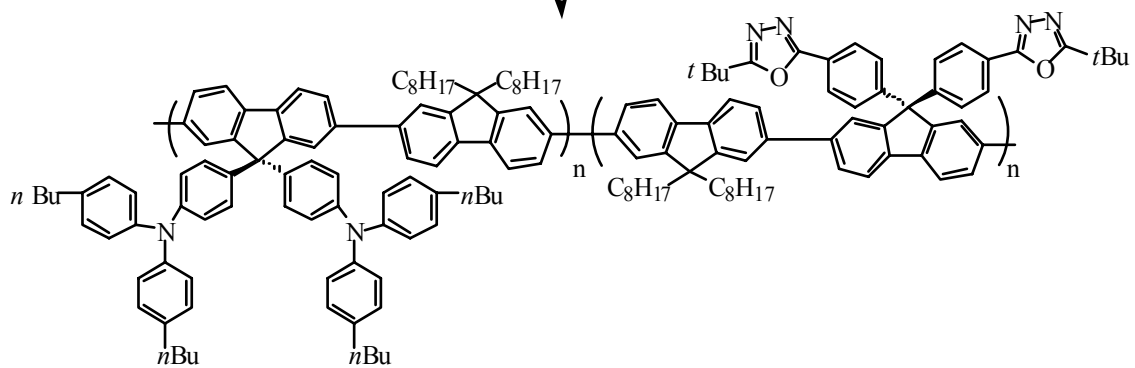
**Appendix D**

Conjugated polymers used in my research.

**PHF**

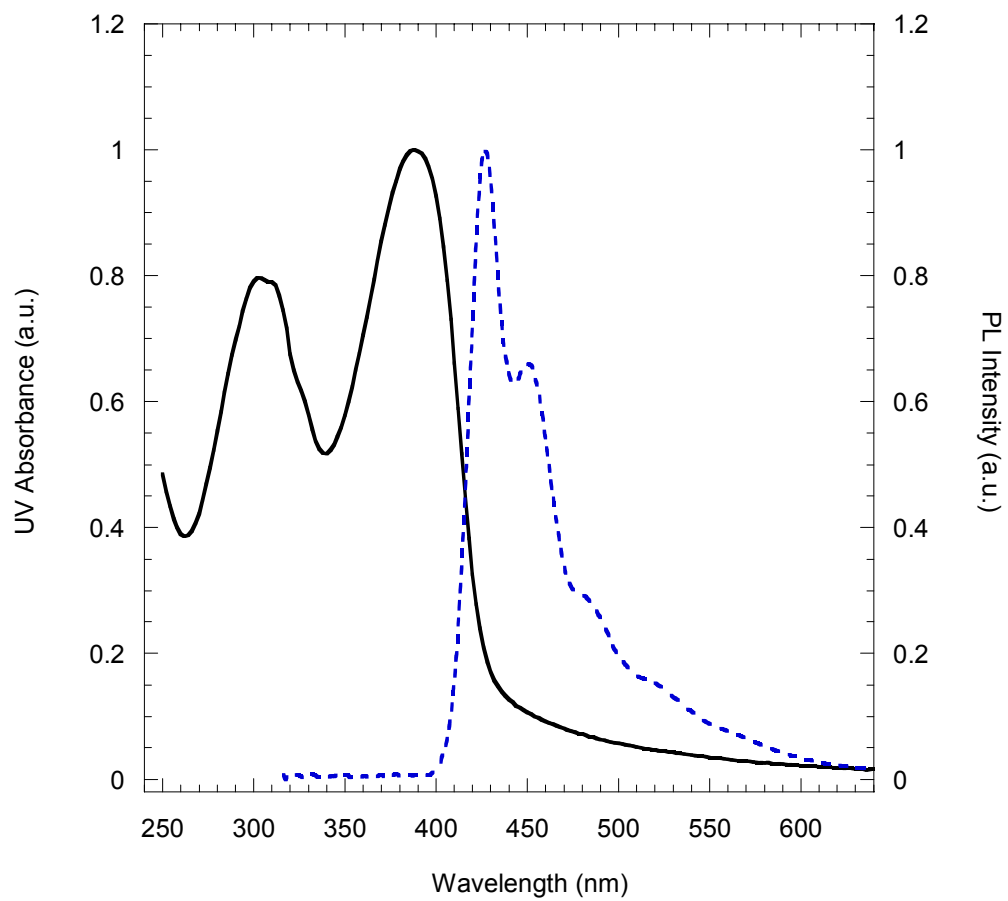






PF-TPA-OXD

PF-TPA-OXD



## Appendix E

- (a) Underlying physical mechanism cartoon depiction (b) Surface plasmon dispersion diagram, polymer interfaced with Au (dashed line), Ag (solid line), and Al (dotted line).

